Atmos. Chem. Phys., 14, 12373–12392, 2014
www.atmos-chem-phys.net/14/12373/2014/
doi:10.5194/acp-14-12373-2014

Atmospheric Chemistry and Physics
Open Access

Measurements of OH and RO_2 radicals at Dome C, East Antarctica

A. Kukui[1,4], M. Legrand[2], S. Preunkert[2], M. M. Frey[3], R. Loisil[5], J. Gil Roca[1], B. Jourdain[2], M. D. King[6], J. L. France[6], and G. Ancellet[1]

[1]Laboratoire Atmosphère, Milieux et Observations Spatiales (LATMOS), UMR8190, CNRS-Université de Versailles Saint Quentin, Université Pierre et Marie Curie, Paris, France
[2]Laboratoire de Glaciologie et Géophysique de l'Environnement (LGGE), UMR5183, CNRS-Université Grenoble Alpes, Grenoble, France
[3]British Antarctic Survey (BAS), Natural Environment Research Council (NERC), Cambridge, UK
[4]Laboratoire de Physique et Chimie de l'Environnement et de l'Espace (LPC2E), UMR6115, CNRS–Université d'Orléans, 45071 Orléans CEDEX 2, France
[5]Division Technique (UPS855) de l'Institut National des Sciences de l'Univers (INSU), Meudon, France
[6]Department of Earth Sciences, Royal Holloway University of London, Egham, Surrey, TW20 OEX, UK

Correspondence to: A. Kukui (alexandre.kukui@cnrs-orleans.fr)

Received: 1 April 2014 – Published in Atmos. Chem. Phys. Discuss.: 6 June 2014
Revised: 15 October 2014 – Accepted: 16 October 2014 – Published: 26 November 2014

Abstract. Concentrations of OH radicals and the sum of peroxy radicals, RO_2, were measured in the boundary layer for the first time on the East Antarctic Plateau at the Concordia Station (Dome C, 75.10° S, 123.31° E) during the austral summer 2011/2012. The median concentrations of OH and RO_2 radicals were 3.1×10^6 molecule cm^{-3} and 9.9×10^7 molecule cm^{-3}, respectively. These values are comparable to those observed at the South Pole, confirming that the elevated oxidative capacity of the Antarctic atmospheric boundary layer found at the South Pole is not restricted to the South Pole but common over the high Antarctic plateau. At Concordia, the concentration of radicals showed distinct diurnal profiles with the median maximum of 5.2×10^6 molecule cm^{-3} at 11:00 and the median minimum of 1.1×10^6 molecule cm^{-3} at 01:00 for OH radicals and 1.7×10^8 molecule cm^{-3} and 2.5×10^7 molecule cm^{-3} for RO_2 radicals at 13:00 and 23:00, respectively (all times are local times). Concurrent measurements of O_3, HONO, NO, NO_2, HCHO and H_2O_2 demonstrated that the major primary source of OH and RO_2 radicals at Dome C was the photolysis of HONO, HCHO and H_2O_2, with the photolysis of HONO contributing ~ 75 % of total primary radical production. However, photochemical modelling with accounting for all these radical sources overestimates the concentrations of OH and RO_2 radicals by a factor of 2 compared to field observations. Neglecting the net OH production from HONO in the photochemical modelling results in an underestimation of the concentrations of OH and RO_2 radicals by a factor of 2. To explain the observations of radicals in this case an additional source of OH equivalent to about (25–35) % of measured photolysis of HONO is required. Even with a factor of 5 reduction in the concentrations of HONO, the photolysis of HONO represents the major primary radical source at Dome C. To account for a possibility of an overestimation of NO_2 observed at Dome C the calculations were also performed with NO_2 concentrations estimated by assuming steady-state NO_2 / NO ratios. In this case the net radical production from the photolysis of HONO should be reduced by a factor of 5 or completely removed based on the photochemical budget of OH or 0-D modelling, respectively. Another major factor leading to the large concentration of OH radicals measured at Dome C was large concentrations of NO molecules and fast recycling of peroxy radicals to OH radicals.

1 Introduction

Atmospheric chemistry in polar regions has gained growing interest over the two last decades due to the discovery of surprisingly high photochemical activity in both Antarctic and Arctic, i.e. at the South Pole (Mauldin et al., 2001; Davis et al., 2001) and at Summit, Greenland (Honrath et al., 1999; Sjostedt et al., 2007). The photochemistry of the boundary layer atmosphere (BL) at these snow covered regions is significantly influenced by the emissions of reactive gases from the snowpack. The emissions are produced by the interaction of solar radiation and photochemically active species in the snowpack (e.g. Grannas et al., 2007 for a review).

At the South Pole (SP) unexpectedly large concentrations of OH radicals in the boundary layer, about 2×10^6 molecule cm^{-3}, were observed for the first time during ISCAT 1998 (Mauldin et al., 2001) and were confirmed in later campaigns (ISCAT 2000, Mauldin et al., 2004; ANTCI 2003, Mauldin et al., 2010). The elevated concentrations of OH radicals were explained by fast recycling of OH radicals from peroxy radicals in presence of large concentrations of NO. The large concentration of NO molecules exceeded free tropospheric concentrations (Davis et al., 2001) and was attributed to the release of NO_x from snowpack (following UV photolysis of the nitrate anion (NO_3^-) on/in snow grains; Jones et al., 2001) and its accumulation in a stable and shallow BL at the SP (Davis et al., 2001, 2004, 2008). The build up of large concentrations of NO_x at the SP was suggested to be enhanced by the continuous sunlight during summer and the location at the bottom of a large air drainage basin (Davis et al., 2004, 2008).

At the SP the major gas-phase net sources of OH and HO_2 radicals were found to be the photolysis of HCHO and H_2O_2. The production of OH radical from O_3 photolysis was found to be less important owing to the small concentration of water at such low temperatures. The photochemical box model for the SP tends to slightly overpredict the concentrations of OH compared to observations, although satisfactorily reproduces the dependence of the concentration of OH on the concentration of NO (Chen et al., 2004; Mauldin et al., 2004). It has to be emphasized that when considering the mixing ratio of ~ 30 pptv of HONO measured at the SP by using mist chamber/ion chromatography method (Dibb et al., 2004) the model overpredicts concentrations of OH radicals at the SP by a factor of 3 to 5 (Chen et al., 2004). It was proposed that the HONO concentrations derived with the mist chamber/ion chromatography method during these campaigns were probably biased by some systematic error (e.g. chemical interference) (Chen et al., 2004).

Conditions favouring the accumulation of large concentrations of NO_x were thought to be specific to the South Pole (24 h sunlight and shallow stable boundary layer), however a larger part of the Antarctic Plateau also experiences elevated concentrations of NO_x despite strongly reduced solar radiation at night and the resulting build up of an unstable convective atmospheric boundary layer. This is supported by airborne observations of large concentrations of NO (Davis et al., 2008; Slusher et al., 2010; Wang et al., 2007) showing that a shallow photochemically active layer is common for large part of Antarctic Plateau atmosphere. However, these airborne measurements of NO_x remain limited in time and space. In addition, although the elevated concentrations of NO_x represent the key factor in the build up of large OH concentrations in the polar BL, the relationship of concentrations of OH with concentrations of NO is non-linear (Mauldin et al., 2004). Thus, an accurate prediction of the concentration of OH radical in other Antarctic regions may be difficult without detailed information on the radical primary production and net losses. These uncertainties in part motivated the OPALE (Oxidant Production in Antarctic Lands and Export) project aiming at a characterization of the oxidative capacity of the BL atmosphere in the region of East Antarctica.

In addition to the monitoring of surface ozone, that was initiated in 2007 at the Concordia station on the East Antarctic plateau (Legrand et al., 2009), two others studies related to the BL photochemistry have been performed at that site prior to the OPALE campaign: the measurements of gas-phase NO concentrations and, for the first time on the Antarctic Plateau, measurements of gas-phase NO_2 concentrations were conducted during summer 2009/2010 by Frey et al. (2013). Frey et al. (2013) revealed that concentrations of NO at Dome C are comparable to those observed at the SP but the ratios $[NO_2] / [NO]$ were found to be significantly larger than calculated, assuming photostationary-state conditions with measured concentrations of O_3 and NO. As a possible explanation Frey et al. (2013) suggested significantly larger peroxy radical concentrations at Dome C than at the SP. The study of Frey et al. (2013) also revealed a distinct diurnal cycle of NO_x that has been attributed to boundary layer stability and the flux of NO_x released from the snowpack both driven by diel changes in solar radiation (France et al., 2011). The second study was dedicated to the measurements of concentrations of HONO during the summer 2010/2011 (Kerbrat et al., 2012) with a long-path absorption photometry (LOPAP) technique. Kerbrat et al. (2012) concluded that the observed large mixing ratio (~ 30 pptv) of HONO would require an unexpectedly large photochemical source of HONO from the snowpack, if the measurements of gas-phase HONO were not biased due to an unknown interference.

In the framework of the OPALE project, aimed at characterization of the oxidative capacity of the atmosphere in the region of East Antarctica (Preunkert el al., 2012), a field campaign was carried out at the top of the high Antarctic Plateau, at Concordia station, from December 2011 to January 2012. The first results of this campaign are presented in several publications accompanying this article, including (Frey et al., 2014) for NO and NO_2, (Legrand et al., 2014) for HONO, and (Preunkert et al., 2014) for HCHO. Here, presented for the first time, are measurements of concentrations of OH and RO_2 radicals conducted on the East Antarctic Plateau at the Concordia station (Dome C). Sources and sinks of these radicals are discussed in the light of concurrent chemical observations made during the campaign, including HONO, NO, NO_2, H_2O_2, HCHO, and O_3, as well as

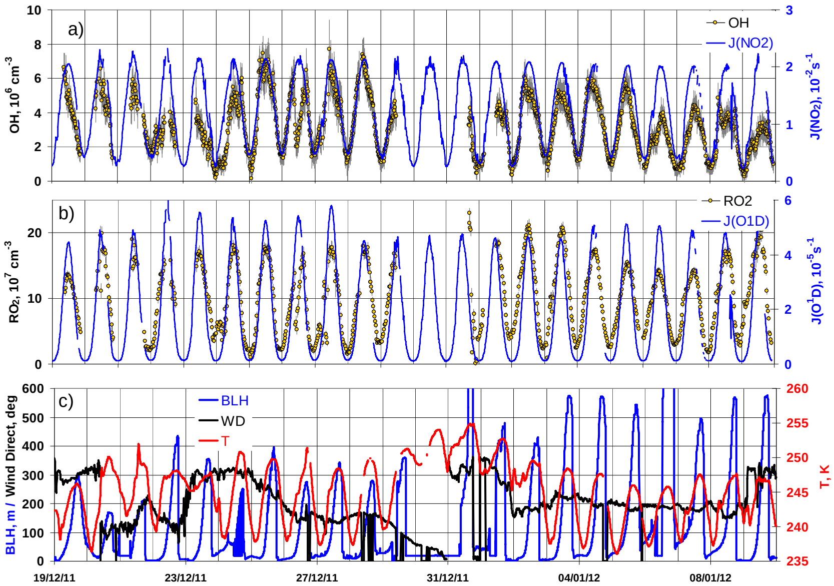

Figure 1. Temporal profiles at Dome C: [OH], $J(NO_2)$ **(a)**; [RO_2], $J(O^1D)$ **(b)**; wind direction, temperature and modelled boundary layer height (BLH) **(c)**.

surface meteorological parameters, physics of the boundary layer and photolysis rates.

2 Methods

Measurements of atmospheric concentration of OH and RO_2 (the sum of hydroperoxy HO_2 and organic peroxy radicals) radicals were conducted from 19 December 2011 to 9 January 2012 at Concordia station (Dome C, 75.10° S, 123.31° E, altitude 3233 m).

The weather at Concordia is dominated by weak katabatic winds ($\sim 3\,m\,s^{-1}$) and clear sky conditions with frequent presence of elevated cirrus clouds. Daylight lasts 24 h with a significant diurnal variation of solar radiation (as shown in Fig. 1a and b for the photolysis rate coefficients for NO_2 and O_3) resulting in a strong diurnal cycle in near-surface temperature (Fig. 1c) and wind speed. During the OPALE campaign the median values of the temperature at a height of 1m and the wind speed ranged from $-36\,°C$ and $2\,m\,s^{-1}$ at 03:00 (all times are local times equivalent to UTC+8 h.) to $-27\,°C$ and $4\,m\,s^{-1}$ at 15:00, respectively. The diurnal solar cycle is responsible for a well defined diurnal cycle of boundary layer structure (Fig. 1c). Starting from about 07:00 in the morning the diurnal heating and upward sensible heat flux (King et al., 2006) drive formation of the convective mixing layer reaching a maximum height of 300–600 m at about 17:00. During the night the boundary layer is stably stratified and confined to a height of several metres. The boundary layer height presented in Fig. 1c comes from the Modèle Atmosphérique Régional (MAR) (Gallée et al., 2014) briefly described in Sect. 2.3.

The measurement site was located in a designated clean-air sector 0.7 km to the south of the main station buildings. During the measurement period the wind direction was predominantly from the south, median value of 180°, with few pollution events (on 19, 31 December and 1 January) due to the wind coming from the station, wind sector of 10–50° (Fig. 1c). The data corresponding to the pollution events were filtered out.

2.1 Radical measurements

Concentrations of OH and RO_2 radicals, as well as sulfuric acid (not shown here), were measured using chemical ionization mass spectrometry (CIMS) (Eisele and Tanner, 1991; Berresheim et al., 2000). Detailed description of the instrument is presented elsewhere (Kukui et al., 2008, 2012; Michoud et al., 2012). Here we briefly present the principle of the method and report details about the setup of the device and working conditions applied during measurements at Dome C.

The concentration of OH radical was measured by titrating atmospherically sampled OH radicals with SO_2 to form H_2SO_4 in a chemical conversion reactor in the presence of water vapour and oxygen (Eisele and Tanner, 1991; Tanner et al., 1997; Berresheim et al., 2000). H_2SO_4 was detected by mass spectrometry as the HSO_4^- ion. The HSO_4^- ion was produced by chemical ionization with NO_3^- in an ion-molecule reactor following the chemical conversion reactor. To distinguish for atmospheric sulfuric acid the chemical titration was performed using isotopically labelled $^{34}SO_2$ leading to the formation of $H_2^{34}SO_4$. The concentration of total peroxy radicals RO_2 was measured by converting RO_2 into OH radicals via reactions with NO injected in the chemical conversion reactor (Reiner et al., 1997) followed by conversion of OH into sulfuric acid.

During measurements at Dome C and similarly to previous measurements in coastal Antarctica at Dumont d'Urville (DDU) (Kukui et al., 2012) the instrument was installed in a shipping container with the chemical conversion reactor fixed to the roof of the container via an interface cap covered with a PTFE sheet. The sampling aperture of the reactor (3 mm diameter) was positioned 50 cm above the roof and about 3 m above the snow surface.

Ambient air was sampled at a volumetric flow rate of 7.4 standard litres (sL) min^{-1} creating turbulent flow in the chemical conversion region of the reactor (Reynolds Number, $Re = 6400$). The turbulent flow conditions minimize possible influence of wind speed on the measurements and ensure fast mixing of reactants. The reactants used for the chemical conversion ($^{34}SO_2$ and NO) and the radical quencher (NO_2) are introduced into the reactor through a set of injectors. NO_2 used as a scavenger removes not only the OH radicals, but also peroxy radicals converting them into HO_2NO_2 and RO_2NO_2 nitrates. The input flow rates of the reactants were similar to those previously used with this instrument (e.g. Kukui et al., 2012), while the sampling flow rate was a factor of 2 smaller than usual. These flow rates were necessary to compensate for the reduced pressure at Dome C (620 hPa) compared to sea-level operation of the instrument, and provided comparable reaction times to previous deployments of this instrument. Switching the reactant flows between the different injectors allows measurements in four different modes: the background mode, two different OH radical measurement modes and the RO_2 radical measurement mode. The two OH measurement modes differ by the time used for the chemical conversion, 4 and 20 ms (Kukui et al., 2008, 2012). Ratio of the signals with the short and the long conversion times may be used as an indicator of an artificial OH formation in the reactor (Kukui et al., 2008).

Measurements of OH, RO_2 and H_2SO_4 were performed by monitoring the peak intensities at $m/z = 62$ (NO_3^-), $m/z = 99$ ($H^{34}SO_4^-$) and $m/z = 97$ ($H^{32}SO_4^-$). The detection of $H^{34}SO_4^-$ and $H^{32}SO_4^-$ corresponds to the measurement of the radicals (OH or RO_2) and H_2SO_4, respectively. The ion peak intensities were measured sequentially resulting in nine measurements of OH and one measurement of RO_2 for every 28 min. Every measurement of OH was derived from 1 min of OH ion signal count and two 30 s background ion signal counts before and after the OH signal measurement. RO_2 was measured at the end of the OH detection sequence by switching on the NO flow to the corresponding injector for a duration of 2 min. To avoid any possible influence of traces of NO on the OH measurements a time delay of 10 min was introduced after switching off the NO flow and before starting the next OH measurement sequence to ensure flushing of the chemical conversion reactor. The measurements of OH and RO_2 radicals were averaged to 15 and 30 min time intervals, respectively.

The concentration of the radicals, $[R]$, is derived from the measured ratio of the $H^{34}SO_4^-$ and NO_3^- ion peak intensities, I_{99} / I_{62}: $[R] = C_R \times \ln(1 + I_{99} / I_{62})$, where C_R is a calibration coefficient determined in calibration measurements by production of a known concentration of OH or RO_2 radicals in a turbulent flow reactor by photolysis of water vapour at 184.9 nm (Heard and Pilling, 2003 and references therein; Faloona et al., 2004; Dusanter et al., 2008). Except for additional thermo-stabilization of a Pen-Ray mercury lamp and a VUV phototube the construction of the calibration cell was the same as previously described in Kukui et al. (2008). The concentration of OH and HO_2 radicals generated in the turbulent flow was calculated from the monitored photon flux and H_2O concentration. For precise control of the concentrations of H_2O at low temperatures the gas manipulation system for the introduction of the mixture of pure air and water vapour into the photolysis reactor was modified by replacing the previously used water trap by a liquid flow controller (Bronkhorst, μ-FLOW series L01, 1.4 g h allowing simulation of typical atmospheric humidities encountered at Dome C (e.g. 50–70 % at −30 °C). During the calibrations at Dome C the previously employed cooled mirror dew-point transmitter used for the humidity measurements in the photolysis reactor was found to be unreliable at low temperatures and was replaced by a capacitive humidity sensor (Vaisala, HMP155) providing more accurate humidity data. The water vapour/air mixture was generated inside the container and introduced to the calibration cell positioned on the roof of the container through a 10 m Teflon tube placed outside of the container, providing the cooling of the calibration gas mixture to the ambient temperature. Despite these modifications frequent difficulties were encountered maintaining stable humidity under conditions of low temperatures at Dome C, limiting calibration accuracy.

The atmospheric concentration of total peroxy radicals RO_2 was measured assuming that the HO_2 and CH_3O_2 radicals represent the major part of all RO_2 radicals at Dome C, i.e. $[RO_2] = [HO_2] + [CH_3O_2]$, with a ratio of $[HO_2] / [RO_2]$ of about 0.7, as informed from the model calculations (see below). The calibration of HO_2 and CH_3O_2 was performed by adding into the calibration cell photolysis reactor either CO or CH_4 converting any OH radical to HO_2 or CH_3O_2, respectively (Hanke et al., 2002; Fuchs et al., 2008). The sensitivity to HO_2 was found to be (15 ± 2) % higher than that for the CH_3O_2.

The overall accuracy of the calibration coefficients was estimated taking into account uncertainties of all parameters used for calculation of the radical concentrations in the photolysis reactor and the precision of the measurements of the ratio I_{99} / I_{62}. The main sources of the calibration uncertainty at Dome C were the estimation of the photon flux (±15 %) and the uncertainty of the measurement of humidity (±30 %). The overall estimated calibration accuracy (2σ) was of 36 % for OH and of 40 % for HO_2. The uncertainty of the measurements of RO_2, accounting for possible variation of the RO_2 composition, was estimated to be of 45 % at Dome C. Accounting for the calibration uncertainties and measurement precision, the overall 2σ uncertainty of the 15 min averaged measurements of OH and RO_2 was estimated to be 40 and 47 % during the daytime and 60 and 50 % during the night time, respectively. The lower limits of detection for OH and RO_2 radicals at signal-to-noise ratio of 3 and a 2 min integration time were 5×10^5 molecule cm^{-3} and 2×10^6 molecule cm^{-3}, respectively.

To avoid possible contamination of ambient air by the SO_2, NO and NO_2 reactants added to the chemical conversion reactor, a trap was set up at the pumps exhaust by using two 100 L cylinders containing zeolites. The cylinders were refilled several times during measurements. Flexible exhaust tube of 30 m length was always placed downwind from the container. When the exhaust tube was intentionally placed upwind and close to the radicals sampling point no effect on radical measurements was detected. Also, no influence of the exhaust on the measurements of NO_x and HONO could be noticed.

2.2 Other measurements

Other chemical measurements conducted at Dome C during the campaign that are relevant to the discussion of sources and sinks of OH and RO_2 radicals include O_3, HCHO, H_2O_2, HONO, NO, NO_2 and photolysis coefficient values. Their median values and ranges are summarized in Table 1, while the detailed discussion of these data and description of the instruments and applied working conditions during the campaign are presented in the corresponding companion papers.

Surface ozone was monitored by UV absorption (Thermo Electron Corporation model 49I) deployed at Dome C since 2007 (Legrand et al., 2009). Atmospheric HCHO measurements were performed with a fluorimetric method using commercial Aerolaser analyzer (model AL-4021) (Preunkert et al., 2014). A fluorimetric two-channel technique was applied for determinations of H_2O_2 (Aerolaser, Model AL2021) (Preunkert et al., 2012).

NO_x was measured with a two-channel chemiluminescence detector with one channel used for NO detection and the other for the sum of NO and NO originating from the quantitative photolytic conversion of NO_2 (Bauguitte et al., 2012; Frey et al., 2013, 2014). The NO_2 and NO measurements are discussed in Frey et al. (this issue). The ratios of NO_2 to NO observed at Dome C during 2011–2012 campaign were up to 3 times larger than in 2009–2010 (Frey et al., 2013) and significantly larger, up to seven times, than the ratios estimated assuming photochemical steady-state (PSS) conditions for NO_x. It is suggested that some part of this inconsistency may be due to unknown interference leading to an overestimation of the NO_2 concentrations (Frey et al., 2014).

The photolysis rate constants, J, were calculated from measurements of "actinic flux" (Madronich, 1987) measured by a Met-Con 2π spectral radiometer with a CCD detector and a spectral range from 285 to 700 nm. The Met-Con Spectral radiometer was calibrated before and after the campaign using a NIST traceable standard 1000 W tungsten halogen lamp. No significant changes were observed in the performance of the spectral radiometer. The spectral radiometer was mounted on a mast of 1m height on the roof of the container used for the radical measurements. A shadow band was fitted to provide a horizontal horizon. Downwelling unweighted radiance over a complete hemisphere, was recorded as a 5 s average for each of the 532 pixels and internally interpolated to a 1 nm resolution over 285–700 nm. The atmospheric photolysis coefficients, J, were calculated using the measured actinic flux along with quantum yields and absorption cross sections from Sander et al. (2011). The principle of using a 2π CCD Met-Con spectral radiometer to accurately determine photodissociation rate constants, J, has been previously demonstrated by Jäkel et al. (2007). Total 4π steradian radiance was calculated by multiplying the downwelling 2π steradian radiance by a value of 1.9. The value of 1.9 is based on measurements of downwelling and upwelling radiance by inverting the spectral radiometer.

HONO was measured with a LOPAP (Heland et al., 2001; Kleffmann et al., 2002) at height of 1m above the snow surface. In spite of the use of the LOPAP, thought to be free of measurement artefacts, mixing ratios of HONO observed at Dome C in December 2011/January 2012 (hourly means of 35 ± 5 pptv, Legrand et al., 2014) are in the same range as previously observed in December 2010/January 2011 (hourly means of 30.4 ± 3.5 pptv) by Kerbrat et al. (2012). As discussed by Legrand et al. (2014), laboratory experiments with irradiated surface snows collected at Concordia reveal that the snowpack may be a very significant source of HONO. It is shown that this source only accounts for a third of the observed HONO mixing ratios at 1 m height at Concordia. Legrand et al. (2014) report tests done both in the field and in the lab that tend to suggest an overestimation of HONO measurements in the range of 10 to 20 pptv due to the presence of HO_2NO_2 in the range of 50–100 pptv in the cold atmosphere at Dome C. This range of HO_2NO_2 mixing ratios is in agreement with the median [HO_2NO_2] of 80 pptv estimated from RO_2 and NO_2 levels measured at Dome C (see Sect. 3.2). Also, as discussed by Legrand et al. (2014), similar levels of HO_2NO_2 were previously observed in Antarctica.

2.3 Model calculations

Observed concentrations of OH and RO_2 were compared with those calculated using a 0-D box model. Photostationary concentrations of OH and RO_2 were calculated by performing numerical integration using a subset from the Master

Table 1. Comparison of measurements at Dome C and at the South Pole.

	Dome C, 75.1° S / 123.3° E 19 December 2011–10 January 2012		SP, ISCAT 1998	SP, ISCAT 2000	SP, ANTCI 2003
	Median (range of median) values	Method (2σ uncertainty)	Median values (16–31 December)[a]		
P, mb	645		688	692	695
T, ° C	−29.6 (−35.8–−26.1)		−29.1	−27.6	−23.9
Wind speed, $m\,s^{-1}$	3.1 (2.3–4.5)		3.2	3.74	4.9
OH, 10^6 molecule cm^{-3}	3.1 (1.1–5.0) 5.0 (at 12 h, $J(O^1D) = 5 \times 10^{-5}\,s^{-1}$) 2.5 (at 5 h, $J(O^1D) = 9 \times 10^{-6}\,s^{-1}$) 3.8 (at 19 h, $J(O^1D) = 9 \times 10^{-6}\,s^{-1}$)	CIMS (40–60 %)	1.7	2.3	1.2
RO_2, 10^7 molecule cm^{-3}	9.9 (2.5–17.0) 17.0 (at 12 h, $J(O^1D) = 5 \times 10^{-5}\,s^{-1}$) 7.9 (at 5 h, $J(O^1D) = 9 \times 10^{-6}\,s^{-1}$) 7.5 (at 19 h, $J(O^1D) = 9 \times 10^{-6}\,s^{-1}$)	CIMS (47–50 %)	–	8.1	–
$J(O^1D)$, $10^{-6}\,s^{-1}$	13.4 (1.2–49)	Spectroradiometer (3 %)	8.9	8.5	8.5
$J(NO_2)$, $10^{-2}\,s^{-1}$	1.3 (0.4–2.1)	Spectroradiometer (6 %)	1.0	1.1	0.8
O_3,ppb	23.7 (22–25)	UV absorption (2 %)	26.1	30	32
NO, ppt (1 m)	77 (46–134)	Chemiluminiscence (40 %)[h]	237	88	76
NO_2, ppt (1 m)	149 (110–239) 16 (7–64)[i]	Photolytic conversion, Chemiluminiscence (200 %)[h]	115[b]	44[b]	38[b]
HONO, ppt	38 (27–44)	LOPAP (5 %)	–	28 (MC/IC)	4.9 (LIF, 10 m) 51(MC/IC, 1 m)[c] 7.3 (LIF, 10 m)[c]
HCHO, ppt	131 (117–153)	Fluorimetry, Aerolaser AL4021 (20 %)	–	105	74
H_2O_2, ppt	166 (128–228)	Fluorimetry, Aerolaser AL2021 (18 %)	–	229	286
$P(O_3)$, ppb day^{-1}	4.7 (0.04–0.34, in ppb h^{-1})[d]		2.2–3.6 [e]	3.2–4.8 [f]	1–3.5 [g]

[a] SP data from Eisele et al. (2008), if no other reference;
[b] estimated assuming PSS ratio NO / $NO_2 = 2$; Davis et al. (2004); Slusher et al. (2002);
[c] median for 1–15 December;
[d] calculated using the measured RO_2 and NO;
[e] Crawford et al. (2001);
[f] Chen et al. (2004);
[g] Davis et al. (2008);
[h] median of relative 2σ errors;
[i] NO_2 estimated assuming PSS conditions for NO_x.

Chemical Mechanism, MCM v3.2 (Jenkin et al., 1997; Saunders et al., 2003; website: http://mcm.leeds.ac.uk/MCM). The subset includes 159 reactions comprising the MCM inorganic section, photochemistry, loss of HNO_3 and RO_2NO_2 by dry deposition and methane chemistry extended with CH_3CHO and CH_3COCH_3. The model ran using the MATLAB package for the entire period from 19 December to 10 January with a 15 min time step and initiated by a 3-day spin-up for the first day. The calculations were constrained by the 15 min averaged measurements of HONO, NO, NO_2, O_3, HCHO, H_2O_2, photolysis coefficients and meteorological parameters. Concentration levels of CO, CH_4, H_2, CH_3CHO, CH_3OOH, CH_3COCH_3 and CH_3COOH, were estimated as described in Sect. 3.2.

The vertical distribution of HONO in the boundary layer was modelled using a 1-D chemistry-transport box model with a vertical distribution of turbulent diffusivity and boundary layer heights calculated by the regional atmospheric MAR model (Modèle Atmosphérique Régional). A detailed description of the model and its validation with respect to observations from the Automatic Weather Station at Dome C is given in Gallée and Gorodetskaya (2008), Gallée et al. (2014) and references therein. The turbulence scheme is based on an E-e scheme and on the Monin–Obukhov Similarity theory (MOST), outside and inside the lowest model layer of MAR, respectively. Similar to calculations performed by Legrand et al. (2014), we used the MAR data obtained with a horizontal resolution of 20 km centred at Dome C; a vertical resolution of 0.9 m up to a height of 23 m above the surface increasing upward to about 50 m at the height of 500 m; 100 vertical levels with a top level at 1 hPa. For the 1-D box model calculations the values of the vertical diffusivity, Kz, were linearly

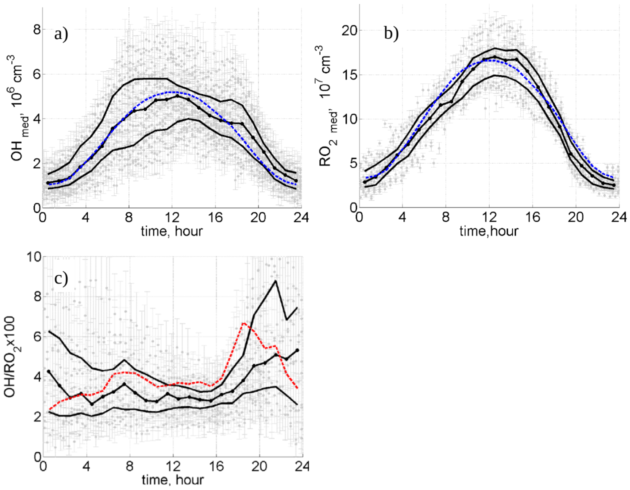

Figure 2. Median diurnal concentration profiles of OH **(a)**, RO_2 **(b)**, [OH] / [RO_2] ratio **(c)**. Solid lines represent the median and quartile levels. Points – 15 min averaged measured values with standard deviations. Blue line in **(a)** and **(b)** represents $J(NO_2)$ in arbitrary units. Red line in **(c)** represents median NO.

interpolated to the vertical grid of 0.1 m from the surface to 5 m, 0.2 m from 5 to 7 m, 0.5 m from 7 to 10 m, around 1 m from 10 to 20 m and then increases up to 120 m at 1200 m height (the BL upper bound was always lower than 1200 m during the OPALE campaign). The boundary layer height is defined by MAR as the height where the turbulent kinetic energy decreases below 5 % of the value at the lowest layer of the model. The calculated boundary layer height profile, as well as measured temperature and wind direction profiles are presented in Fig. 1.

3 Results and discussion

3.1 Presentation of the measurements of OH and RO_2 radicals

Measurements of the concentration of OH and RO_2 radicals are presented in Figs. 1 and 2. The radical concentrations exhibited clear diurnal profiles driven by the solar radiation cycle and ranged from 3×10^5 to 7.5×10^6 and from 1×10^7 to 2×10^8 for OH and RO_2, respectively, in units of molecule cm^{-3}. As shown in Fig. 2, the diurnal profiles of OH and RO_2 radicals follow the diurnal variation of the NO_2 photolysis coefficient, $J(NO_2)$. At the same time, one can notice some deviation of the diurnal concentration profiles of OH and RO_2 from the $J(NO_2)$ profile with larger concentrations for OH and lower for RO_2 in the afternoon. This is reflected in the diurnal profile of the ratio of [OH] to [RO_2] (Fig. 2c) which shows a diurnal profile with lower values of [OH] / [RO_2] during the day and factor of ~ 2 larger in the afternoon. Notably, the [OH] / [RO_2] diurnal profile correlates with the daily profile of the concentration of NO (Fig. 2c).

The median concentrations of RO_2 and OH radicals measured at Dome C are compared to those observed at the South Pole in Table 1. At Dome C the $J(O(^1D))$ daily median values at 05:00 and 19:00 ($9 \times 10^{-6}\,s^{-1}$) are similar to median $J(O(^1D))$ observed at the SP ($(8.5–9.0) \times 10^{-6}\,s^{-1}$). Comparing the corresponding concentrations of OH radical one can see that the median values at Dome C are close to that observed at the SP for 05:00 and somewhat higher at 19:00, 2.5×10^6 and 3.8×10^6, respectively, compared to 2.3×10^6 at the SP during ISCAT 2000. The concentrations of NO at the SP were similar to the observed at Dome C, 88 and 77 pptv, respectively.

As seen in Fig. 3, the concentrations of both OH and RO_2 correlate linearly with $J(NO_2)$ with about 60 and 80 % of the variability of OH and RO_2, respectively, explained by the variability of $J(NO_2)$. The relationship of [OH] with $J(O(^1D))$, although with a large scattering as in the case with $J(NO_2)$, was close to a power-law dependence with an exponent of ~ 0.5 in accordance with a typical close to quadratic dependence of $J(O(^1D))$ on $J(NO_2)$ observed at Dome C. As seen from the colour coding in Fig. 3 by concentration of NO of the graph points, there is an obvious correlation with [NO], positive for [OH] and negative for [RO_2]. In fact, about 80 % of the [OH] / [RO_2] variability may be explained by the linear correlation with [NO] (Fig. 3c).

The important role of NO in controlling the concentrations of OH and RO_2 is seen in Fig. 4 where [OH] and [RO_2] are normalized by $J(NO_2)$ to remove the dependence on solar radiation and plotted against [NO]. For concentrations of NO of up to ~ 150 pptv the concentration of OH rises and then levels off, while [RO_2] exhibits the reverse dependence on [NO]. These dependences are very similar to those observed at the SP (Figs. 2 and 7 in Mauldin et al., 2004) and can be explained in a similar way: when the concentration of NO is small, the concentration of OH increases due to the enhanced recycling from RO_2 until the losses of RO_2 and OH in reactions with NO_2 become important compared to other loss processes and therefore compensate the enhanced OH formation (see below for further discussion).

Owing to an approximate linear correlation of [HONO] with [NO] observed at Dome C (Legrand et al., 2014) together with a approximately linear relation between $J(HONO)$ and $J(NO_2)$ the dependence of the concentrations of OH and RO_2 on $J(HONO)$ and HONO is very similar to that on $J(NO_2)$ and [NO] presented in Figs. 3 and 4, implying the concentration of HONO also could be an important parameter controlling the radical variability.

3.2 Radical sources and sinks

The sources and sinks of OH and RO_2 radicals at Dome C were calculated using the radical field measurements and other available relevant observations presented in Table 1.

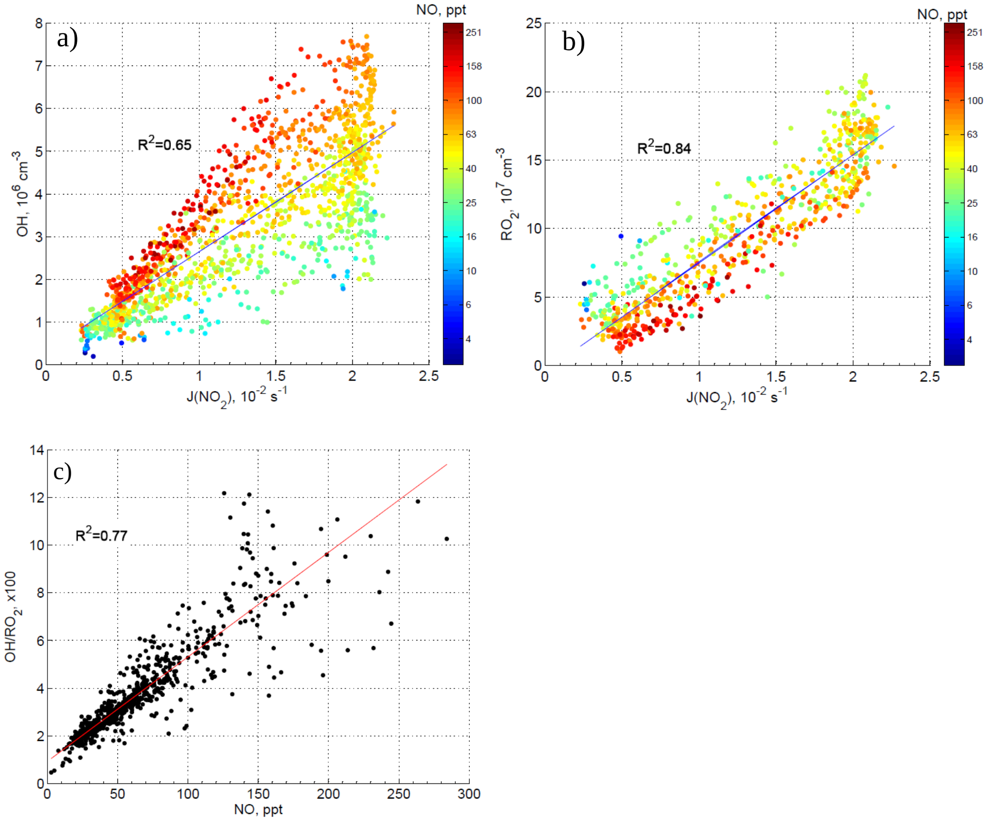

Figure 3. Correlations of [OH] **(a)** and [RO_2] **(b)** with $J(NO_2)$ and of [OH] / [RO_2] with [NO] **(c)**.

Some of the key species involved in the radical production and losses, namely CO, CH_4 and H_2, were not measured. For CO, a mixing ratio of 40 ± 4 ppbv was assumed referring to the value observed at the South Pole (Novelli and Masarie, 2013). Similar mixing ratios of CO for the period of December–January have been measured during ISCAT 2000 at the SP (Davis et al., 2004) and at DDU (Preunkert et al., 2012). For methane and H_2 mixing ratios the values of 1.8 ppmv (Steele et al., 2002) and 520 ppbv (Steele et al., 2003) are adopted, respectively, based on measurements made at other Antarctic sites.

Measurements of acetaldehyde are sparse in Antarctic regions. As discussed by Legrand et al. (2012), at the coastal site of DDU an acetaldehyde background mixing ratio close to 80 pptv can be assumed, though this value may be highly variable over the Southern ocean (5 to 50 pptv). Hamer et al. (2007) reported a mixing ratio of CH_3CHO of 60 pptv at the SP. In our calculations we used a value of 60 pptv with an uncertainty of 20 %. Methyl hydroperoxide (CH_3OOH), acetic acid (CH_3COOH) and acetone (CH_3COCH_3) were also considered in our calculations. CH_3OOH was estimated from observations of H_2O_2 made at Dome C (mean value of 166 pptv, see Table 1) and assuming that it represents 40 ± 10 % of H_2O_2 as reported by Frey et al. (2005) at the SP. For CH_3COCH_3 a typical mixing ratio of 130 ± 30 pptv was used on the basis of observations made at the SP (Hamer et al., 2007). For CH_3COOH, Legrand et al. (2012) measured 60–70 pptv at Dome C between November and February.

The calculated rates of radical sources and sinks are presented in Fig. 5 and Table 2. Based on available measurements the major primary radical source is the photolysis of HONO (1), with other net sources, namely, photolysis of HCHO (7), H_2O_2 (2), O_3 (3) and CH_3CHO (8) being less important and contributing altogether less than 30 % of the net radical production (the numbering of the reactions is according to the Table 2). It is important to emphasize here that, as detailed in Sect. 2.2, the HONO data used in these calculations are thought to be biased by the presence of HO_2NO_2 (Legrand et al., 2014). Since the raw HONO concentration data cannot be accurately corrected for this measurement artefact, we consider in the following discussion (Sects. 3.4 and 3.5) several scenarios for HONO mixing ratios.

The recycling of OH and RO_2 radicals proceeds mainly via the reactions of HO_2 with NO (5) and of OH with CO (10) and CH_4 (11), with the production rate of OH from $HO_2 + NO$ being about half of the generation rate of OH via the photolysis of HONO. Although being less important, additional regeneration of RO_2 by the reactions of OH with HCHO, CH_3CHO, O_3 and H_2 (12–15) remain significant.

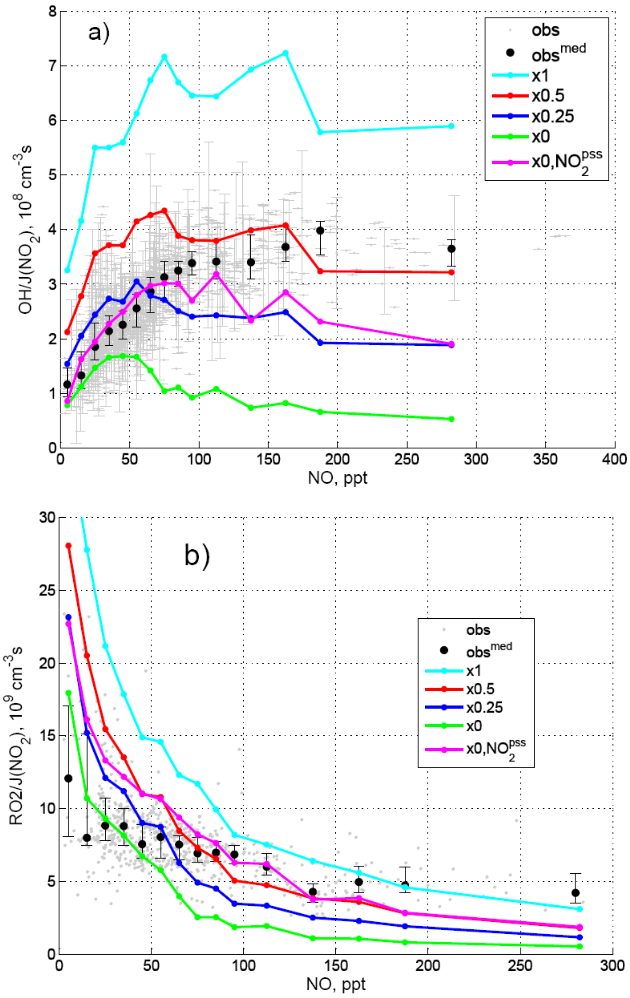

Figure 4. Normalized concentrations of OH **(a)** and RO_2 **(b)** versus measured concentrations of NO. Grey and black points represent observations; coloured lines – MCM calculations with [HONO] multiplied by a factor presented in figure legends (x0 corresponds to estimated steady-state HONO concentrations). Magenta – PSS [HONO] and [NO_2] is calculated by assuming PSS [NO_2] / [NO] ratio.

Net loss of the radicals proceeds mainly via the reactions OH+NO_2 (18), $RO_2 + NO_2$ (24) and radical cross reactions $OH + RO_2$ (20) and $RO_2 + RO_2$ (25). Note that radical cross reactions become particularly important during the day when concentration of RO_2 is large (Table 2). Reactions of OH with NO, HONO, RO_2NO_2 and HNO_3 contribute together about 16 % to the radical net losses. The contribution of the reaction of $HO_2(H_2O)$ with NO_2 (Li et al., 2014) to the RO_2 losses is estimated with the rate constants given in Legrand et al. (2014) to be less than 1 %.

As the losses of OH and RO_2 via the reactions with NO_2 may be overestimated due to unknown interference in the NO_2 measurements (Frey et al., 2014) we also present in the Table 2 (values in parenthesis) the radical losses for [NO_2] estimated assuming PSS conditions for NO_x. In this case the net daytime radical losses are dominated by the radical cross reactions $RO_2 + RO_2$ (25) and $OH + RO_2$ (20).

According to the above mechanism derived from the field observations, the sum of peroxy radicals RO_2 is composed predominantly of HO_2 and CH_3O_2, $[RO_2] = [HO_2] + [CH_3O_2]$. The ratio of [$HO_2$] to [$RO_2$] which was required for calculating the radical sources/sinks was estimated using steady-state calculations accounting for all identified sources and sinks of HO_2 and CH_3O_2. The resulting value of [HO_2] / [RO_2] is $0.67 \pm 0.05(1\sigma)$ and is close to the ratio of 0.73 estimated by only accounting for the production of RO_2 in the reactions of OH radical with CO and CH_4 and the loss of RO_2 via reactions of RO_2 with NO.

Concentrations of peroxy nitrates ($CH_3O_2NO_2$ and HO_2NO_2) involved in radical loss reactions (see Table 2) were not measured at Dome C but were estimated assuming steady-state conditions and accounting for their losses via photolysis, the reaction with OH, thermal decomposition and a surface deposition of $7 \times 10^{-5}\,s^{-1}$ (Slusher et al., 2002). The calculated mixing ratios of HO_2NO_2 and $CH_3O_2NO_2$ were ~ 80 and ~ 20 pptv, respectively. These mixing ratios of HO_2NO_2 are somewhat higher than [HO_2NO_2] of 40–60 pptv observed at the South Pole (Slusher et al., 2010) under conditions of significantly lower [NO_2] (estimated at SP from NO observations assuming steady-state). Assuming the steady-state NO_2 concentrations at Dome C the estimated mixing ratios of HO_2NO_2 and $CH_3O_2NO_2$, are significantly lower: ~ 10 and ~ 3 pptv, respectively. In the work presented here the calculated steady-state concentrations of peroxy nitrates were used to estimate the effective loss rates of RO_2 radicals in the reactions with NO_2 by accounting for the regeneration of RO_2 via RO_2NO_2 thermal decomposition.

The mechanism presented above of the radical production and loss is supported by examination of specific correlations. The major sources of OH radical, both the photolysis of HONO and the recycling from HO_2, are expected to correlate with photolysis rates. Hence, the observed close to linear correlation between [OH] and $J(NO_2)$ or J(HONO) (Fig. 3) tends to support the importance of these two mechanisms of the production of OH radical. However, the correlation of [OH] with $J(NO_2)$ explains only about 60 % of [OH] variability, while an additional source of [OH] variability may come from the variability of [HONO] and/or [NO] as it can be seen from Fig. 3. To account for the variability of [HONO] and [NO], in Fig. 6 we plotted [OH] against production rates of OH radical via photolysis of HONO, (P_{HONO}), and via reaction of HO_2 with NO, (P_{HO_2+NO}). The variability of P_{HO_2+NO} and P_{HONO} then explain ~ 80 % of the variability of OH.

Table 2. Sources and sinks of OH and RO_2 radicals estimated from the measurements available at Dome C*.

		Median rate, 10^5 molecule cm^{-3} s^{-1}		
		Daily	Noon	Midnight
	Net OH sources			
1	$HONO + h\upsilon \rightarrow OH + NO$	14.2 (0.5)	21.8 (0.6)	4.7 (0.2)
2	$H_2O_2 + h\upsilon \rightarrow OH + OH$	0.9	2.1	0.1
3	$O_3 + h\upsilon \rightarrow O(^1D) \rightarrow OH + OH$	0.3	1.7	0.0
4	$CH_3OOH + h\upsilon \rightarrow HO_2 + OH$	0.2	0.4	0.0
	Recycling $RO_2 \rightarrow OH$			
5	$HO_2 + NO \rightarrow OH + NO_2$	8.3	11.6	2.2
6	$HO_2 + O_3 \rightarrow OH + 2O_2$	0.4	0.6	0.1
	Net RO_2 sources			
7	$HCHO + h\upsilon \rightarrow 2HO_2 + CO$	2.1	3.7	0.4
8	$CH_3CHO + h\upsilon \rightarrow HO_2 + CH_3O_2 + CO$	0.9	2.1	0.2
9	$CH_3OOH + h\upsilon \rightarrow HO_2 + OH$	0.2	0.4	0.03
	Recycling $OH \rightarrow RO_2$			
10	$CO + OH \rightarrow HO_2 + CO_2$	5.9	7.8	1.9
11	$CH_4 + OH \rightarrow CH_3O_2 + H_2O$	2.3	3.3	0.7
12	$HCHO + OH \rightarrow HO_2 + CO$	1.0	1.1	0.3
13	$CH_3CHO + OH \rightarrow CH_3CO_3$	0.8	1.1	0.3
14	$O_3 + OH \rightarrow HO_2 + O_2$	0.6	0.7	0.2
15	$H_2 + OH \rightarrow HO_2 + H_2O$	0.5	0.8	0.2
16	$CH_3OOH + OH \rightarrow CH_3O_2 + H_2O$	0.3	0.5	0.1
17	$H_2O_2 + OH \rightarrow HO_2 + H_2O$	0.1	0.3	0.0
	Net radical losses			
18	$OH + NO_2 \rightarrow HNO_3$	1.9 (0.3)	2.2 (0.3)	1.1 (0.3)
19	$OH + NO \rightarrow HONO$	0.5	0.6	0.2
20	$OH + RO_2 \rightarrow$ products	0.4	1.0	0.0
21	$OH + RO_2NO_2 \rightarrow$ products	0.4 (0.05)	0.5 (0.06)	0.1 (0.02)
22	$OH + HONO \rightarrow H_2O + NO_2$	0.1 (0.0)	0.2 (0.0)	0.1 (0.0)
23	$OH + HNO_3 \rightarrow H_2O + NO_3$[a]	0.0	0.0	0.0
24	$RO_2 + NO_2 \rightarrow RO_2NO_2 \rightarrow$ products	1.9 (0.3)	2.4 (0.3)	1.2 (0.3)
25	$RO_2 + RO_2 \rightarrow$ products	0.7	2.1	0.1
26	$RO_2 + OH \rightarrow$ products	0.4	1.0	0.0
	$\sum$OH sources	24.2 ± 2.1[b]	38.3 ± 3.2	7.1 ± 0.7
		(10.6 ± 0.2)	(17.1 ± 0.3)	(4.3 ± 0.1)
	$\sum$OH losses	14.8 ± 4.6	20.3 ± 3.6	5.1 ± 1.2
		(12.9 ± 1.8)	(17.9 ± 2.2)	(4.3 ± 0.9)
	Δ	9.4 ± 5.0	17.9 ± 4.8	2.1 ± 1.4
		(-2.4 ± 2.7)	(-0.8 ± 3.8)	(-1.7 ± 1.2)
	$\sum RO_2$ sources	14.6 ± 1.8	21.9 ± 2.3	4.2 ± 0.9
	$\sum RO_2$ losses	11.7 ± 4.6	17.7 ± 7.2	3.5 ± 1.6
		(10.2 ± 2.1)	(15.6 ± 3.3)	(2.7 ± 0.8)
	Δ	2.9 ± 5.0	4.2 ± 7.6	0.7 ± 1.9
		(4.4 ± 2.8)	(6.3 ± 4.0)	(1.5 ± 1.2)
	$\sum RO_2$ and OH net sources	18.7 ± 0.6	32.3 ± 0.9	5.5 ± 0.1
		(5.1 ± 0.3)	(11.1 ± 0.7)	(0.9 ± 0.1)
	$\sum RO_2$ and OH net losses	6.4 ± 5.9	10.1 ± 7.1	2.7 ± 1.7
		(3.0 ± 0.8)	(5.6 ± 1.1)	(1.1 ± 0.4)
	Δ	12.3 ± 6.0	22.2 ± 7.2	2.7 ± 1.7
		(2.1 ± 0.9)	(5.5 ± 1.3)	(-0.1 ± 0.5)
	$P_{pr}^{net}(OH) = \sum$net OHt sources – $\sum$net OH losses	12.2 ± 4.2	21.4 ± 3.0	3.4 ± 0.8
		(0.4 ± 0.3)	(2.7 ± 0.5)	(-0.3 ± 0.2)
	$R_{net}(OH \rightarrow RO_2) = \sum (OH \rightarrow RO_2) - \sum (RO_2 \rightarrow OH)$	2.8 ± 2.7	3.5 ± 3.8	1.4 ± 1.1
	$P_{pr}^{net}(RO_2) = \sum$ net RO_2 sources – $\sum$ net RO_2 losses	0.15 ± 4.2	0.74 ± 6.6	-0.7 ± 1.5
		(1.7 ± 0.8)	(2.8 ± 1.2)	(0.2 ± 0.4)

* Values in parentheses correspond to NO_2 and HONO estimated assuming PSS;
[a] HNO_3 of (100 ± 30) ppt was assumed (Slusher et al., 2010);
[b] 1σ uncertainty estimated with accounting for measurement uncertainties.

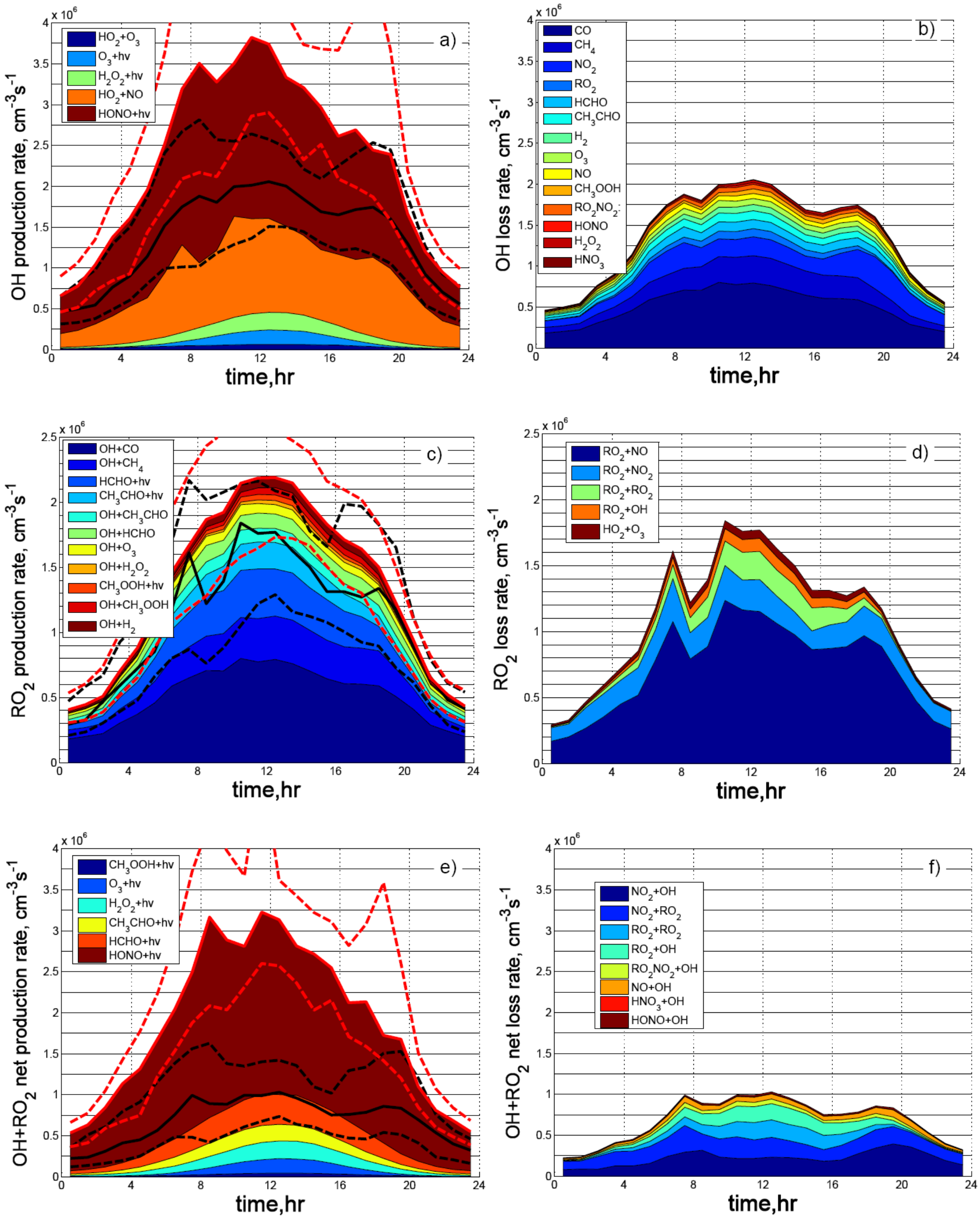

Figure 5. Median diurnal production and loss rates of OH **(a, b)**, RO_2 **(c, d)**; net production and loss rates of radicals **(e, f)**. Solid red and black lines represent the total production and loss rates, respectively. Dashed lines correspond to corresponding quartiles.

3.3 Photochemical budget of radicals

According to the calculated sinks of OH and RO_2 radicals their lifetimes were less than 3 and 100 s, respectively. The timescales for the variability of atmospheric parameters at Dome C (boundary layer height and vertical diffusivity, solar radiation, NO_x concentration etc.) were typically significantly larger, more than 10 min. Hence, assuming validity of a steady-state approximation for OH and RO_2, their sources and sinks should be balanced. However, as shown in Fig. 5 and Table 2, on the basis of observations the sum of the radical production rates exceeds by about (40–90) and 25 % the sum of loss rates for OH and RO_2 radicals, respectively. Considering the primary sources and net sinks of the sum of OH and peroxy radicals, the measured primary radical production

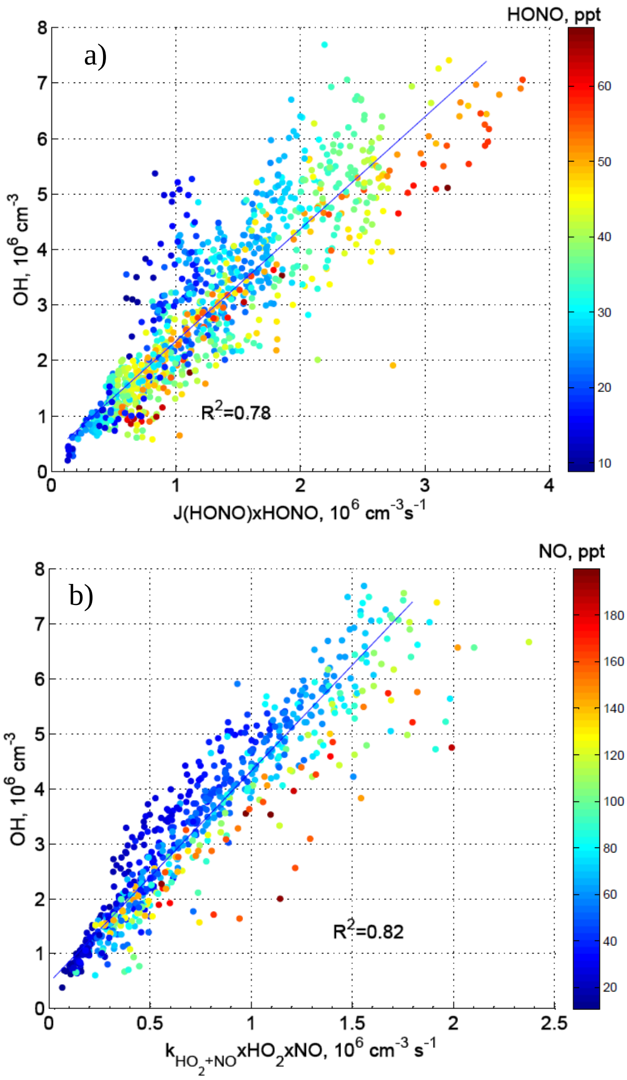

Figure 6. Correlation of measured [OH] with production rates of OH radical by photolysis of HONO, P_{HONO} **(a)**, and via reaction HO_2+NO, P_{HO_2+NO} **(b)**.

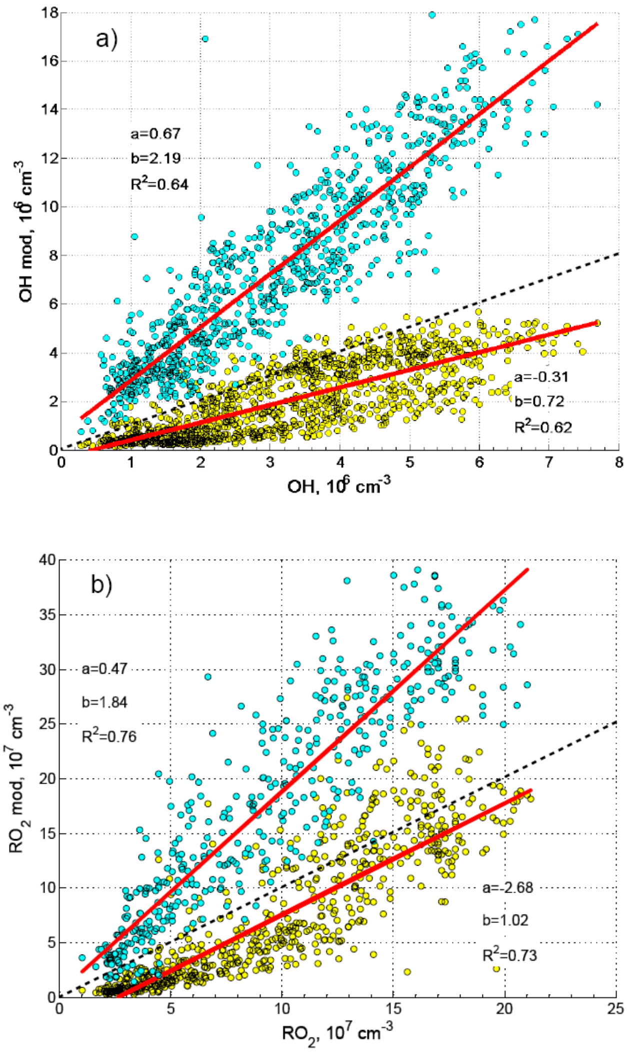

Figure 7. Modelled with the 0-D model vs. measured [OH] **(a)** and [RO_2] **(b)**: yellow – with PSS estimated HONO; blue – with measured [HONO]. Coefficients a, b correspond to intercept and slope, respectively. Black lines correspond to linear dependences with $a = 0$ and $b = 1$.

is larger than their measured total removal rate by a factor of 2 and 3 for midnight and noon times, respectively.

A similar result of the budget analysis follows from the comparison of the net OH and RO_2 production rates, i.e. from the difference of the sum of their primary sources and the sum of their net removal, and the total rate of the radical recycling. Under steady-state conditions the net production (or removal) rate of OH, $P_{\mathrm{pr}}^{\mathrm{net}}(\mathrm{OH})$, should be compensated by the net removal (or production) rate of RO_2, $-P_{\mathrm{pr}}^{\mathrm{net}}(\mathrm{RO_2})$, and equal to the net recycling rate of OH to RO_2 (or RO_2 to OH), R^{net} (OH→RO_2), (see Table 2):

$$P_{\mathrm{pr}}^{\mathrm{net}}(OH) = R^{\mathrm{net}}(\mathrm{OH} \rightarrow \mathrm{RO_2}) = -P_{\mathrm{pr}}^{\mathrm{net}}(\mathrm{RO_2}).$$

However, as seen in Table 2, according to the field measurements the net primary production rate of OH significantly exceeds both the OH to RO_2 recycling and the net RO_2 removal rates. At the same time, the net conversion rate of OH to RO_2 is not compensated by the measured net removal rate of RO_2. This interpretation shows in a different way the same result as Fig. 5: for both OH and RO_2 radicals the measured radical production rate exceeds their loss rate, although for RO_2 the difference is less significant.

The observed imbalance between radical production and loss could result from underestimated or unaccounted radical losses, as well as from overestimated radical sources. As the main radical loss processes identified at Dome C were the reactions of radicals with NO_2 and radical cross reactions the underestimation of the radical losses could be related to an underestimation of measured concentration of NO_2 and/or concentrations of OH and RO_2 radicals. The underestimation of the radical concentrations by a factor of 2 is well outside the estimated uncertainties for the measurements of OH and RO_2, although we can not completely exclude some unknown error in the radical calibration procedure.

Considering the possibility of the underestimation of the concentration of NO_2, sensitivity analysis shows that increasing of the concentrations of NO_2 by a factor of ~ 3 would result in a fair agreement of the model with the observations. However, as the observed $[NO_2] / [NO]$ ratios at Dome C are already very high it is very unlikely that measured NO_2 was underestimated. As discussed in Frey et al. (2013, this issue) the ratios of $[NO_2] / [NO]$ observed at Dome C are not consistent with other observations available at Dome C. Accounting for the photolysis of NO_2 and conversion of NO to NO_2 in the reactions with measured $[RO_2]$ and $[O_3]$ results in the ratio of $[NO_2]$ to [NO] about a factor of 7 lower compared to the measured values suggesting that there is a missing mechanism of the conversion of NO to NO_2. An explanation evoking an underestimation of the measured RO_2 can be excluded, because the concentrations of RO_2 radicals needed to explain the observed ratio of $[NO_2] / [NO]$ would be a factor of 20 larger than measured. Another possibility would be an additional conversion of NO to NO_2 in presence of halogens (e.g. ClO, BrO, IO) as was found at other polar sites, e.g at the coastal site of Halley (Bauguitte et al., 2012). However, to explain the observed ratio of $[NO_2] / [NO]$ at Dome C a very large concentration of halogen species would be required, about 60 pptv in case of BrO and even higher for ClO. Such a large halogen mixing ratio is contradicted by measurements of BrO at Dome C, i.e. Frey et al. (2014) report the BL mixing ratios of BrO of ~ 2 pptv. Hence, we conclude that either there is some unknown mechanism of NO to NO_2 conversion, or there was some interference affecting the NO_x measurements.

The analysis performed here of the radical chemistry at Dome C could be affected in both cases: the missing NO_x chemistry could interfere with chemistry involving OH and RO_2, i.e. by shifting the ratio $[RO_2] / [OH]$ towards OH, like in the case of efficient halogen chemistry at Summit, Greenland (Liao et al., 2011), while biased measurements of NO_x could affect the calculated radical losses and interconversion rates. Further speculations about possible impact of an unknown NO_x regulating mechanism on the OH and RO_2 chemistry are not feasible at this stage. Concerning possible interference in NO_x measurements, any correction consisting in a reduction of NO_2 would result in weaker radical losses and, hence, even larger overestimation of the radical sources. As shown in Table 2 the assumption of steady-state NO_2 concentrations lead to a significant overestimation of the net radical production for RO_2 and $(RO_2 + OH)$ even when neglecting net OH production by the photolysis of HONO. For OH budget, neglecting the net OH production by the HONO photolysis would lead to an underestimation of the OH production.

Considering the possibility of some overestimation of the OH radical production rate and independent of discussions carried out elsewhere (Legrand et al., 2014), one can see from Fig. 5 and Table 2 that among all the measured radical sources only the photolysis of HONO is large enough to explain, in case of its overestimation, the observed imbalance. In the following section we compare the observed concentrations of OH and RO_2 with model predictions to test the sensitivity of the modelled [OH] and $[RO_2]$ to the concentration of HONO.

3.4 Comparison with 0-D model: sensitivity to HONO

The simulations of concentration profiles of OH and RO_2 were conducted with different constraints on the concentration of HONO: taken as measured by LOPAP, the LOPAP measurements reduced by factors 2, 4, and estimated accounting for HONO production in HO+NO and HONO removal by photolysis assuming PSS conditions. The calculations were constrained with measured concentrations of NO_2 unless specifically stated that PSS-derived NO_2 was used. The modelled concentrations of OH and RO_2 radicals are presented in Figs. 7 and 8. Accounting for all radical sources including the photolysis of HONO leads to about a factor of 2 overestimation for modelled $[RO_2]$ and [OH] with moderate correlation of the calculated and observed concentrations of OH and RO_2 radicals. Assuming HONO at PSS leads to an underestimation of [OH] and $[RO_2]$ with a ratio of modelled to observed concentrations (M / O) of about 0.5 and a distinct difference between modelled and observed diurnal profiles (Fig. 8), with better agreement during the daytime. As shown in Fig. 8 the M / O for OH, RO_2 and their ratio become close to 1 by decreasing [HONO] from the measured to concentrations reduced by a factor of 4.

Similar to the approach adopted at the SP (e.g. Davis et al., 2004) we have tested the model assuming PSS HONO concentrations and using concentrations of NO_2 calculated by assuming photostationary ratio of $[NO_2] / [NO]$ calculated from the observed concentrations of NO, O_3 and RO_2. In this case, similar to the SP results, we obtain quite a good description for [OH], although with up to a factor of 1.5 overestimation of $[RO_2]$ and $[RO_2] / [OH]$ ratio at noon (Fig. 8).

Another insight on the relationship between the calculated concentrations of radicals and [HONO] can be gained by comparing the dependencies of observed and calculated [OH] and $[RO_2]$ normalized by $J(NO_2)$ on [NO] (Fig. 4). The model clearly shows that neglecting HONO photolysis and using constraints by measured concentrations of NO_x leads to a clear disagreement with observations. In this case, the calculated roll-off of normalized [OH] starts at a mixing ratio of NO of about 50 pptv (Fig. 4a) as a consequence of fast losses due to large $[NO_2]$ and the lack of additional OH production at higher concentrations of NO_x. When it is assumed that measurements of HONO are correct, [OH] and $[RO_2]$ are overestimated by a factor of almost two in the

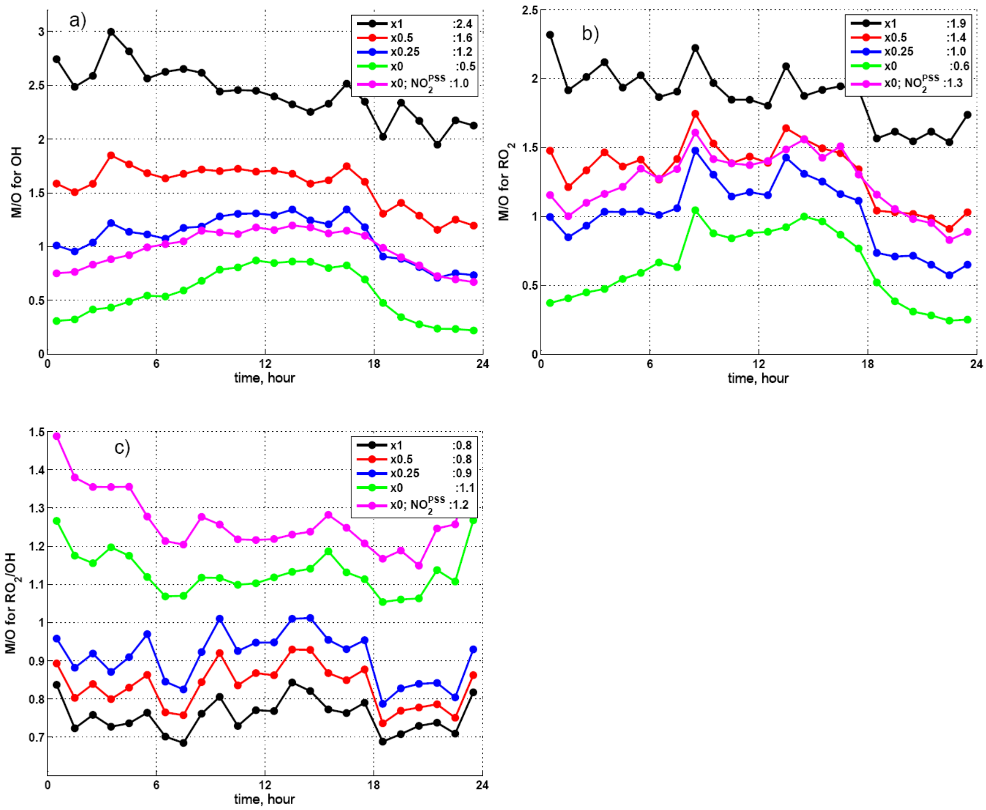

Figure 8. Median diurnal model/observation ratios for [OH] **(a)**, [RO_2] **(b)** and [RO_2] / [OH] **(c)** at [HONO] = 1, 0.5, 0.25, of measured. The "x0, NO_2^{PSS}" curves correspond to the model with [HONO] estimated assuming PSS and [NO_2] calculated assuming [NO_x] at PSS. Numbers in legends represent diurnal median M / O ratios.

whole range of observed [NO]. A better description by the model is achieved either when reducing the HONO concentrations by a factor of 4 or by neglecting HONO and using [NO_2] calculated assuming PSS for NO_x (see also Fig. 8). In the latter case, the model underestimates the concentrations of radicals by 30–40 % at large [NO], although the number of observations at large concentrations of NO (>200 pptv) is limited.

Considering diurnal profiles of the M / O ratio presented in Fig. 8 one can see that although reducing the production rate of OH from the photolysis of HONO by reducing the concentration of HONO improves the agreement between the model and the observations, the diurnal profiles of the M / O ratio become more distinct indicating that a simple reduction of [HONO] cannot provide a satisfactory description for the diurnal concentration profiles of OH and RO_2. Thus, either some chemical mechanism is missing in the model and its effect on the M / O ratio becomes stronger at reduced rates of OH production or, the overestimation of the OH production rate is dependent on time of day (see discussion of effects related to BL diffusivity in Sect. 3.5). In fact, median values of the time-dependent correction of [HONO] necessary to provide agreement between calculated and observed radical concentrations can be estimated by solving radical sources and losses balance equations for the concentration of HONO. As shown in Fig. 9, for the OH radical budget the balance is achieved by reducing P_{HONO} by a factor of 3 during the day with a smaller correction required during the night. Balancing the budget of primary production and net removal rates of radicals requires neglecting the photolysis of HONO during the day and reducing it to a quarter of its original value during the night time. According to a sensitivity analysis to different measured parameters the calculated to observed [HONO] ratios, $[HONO]_{calc}$ / $[HONO]_{obs}$, are most sensitive to the concentrations of NO_2 and OH, RO_2 radicals. By assuming the PSS-derived NO_2 concentrations, the balance for the OH radical budget is achieved by reducing P_{HONO} by a factor of 5, while for RO_2 and the sum of RO_2 and OH the radical production is overestimated even if the net source from HONO photolysis is neglected.

3.5 Comparison with 1-D model

It follows from the analysis presented above in Sect. 3.4 that the concentrations of HONO observed at Dome C were probably too large and not compatible with the measurements of OH and RO_2. Legrand et al. (2014) give indications of possible interference from HO_2NO_2 leading to an overestima-

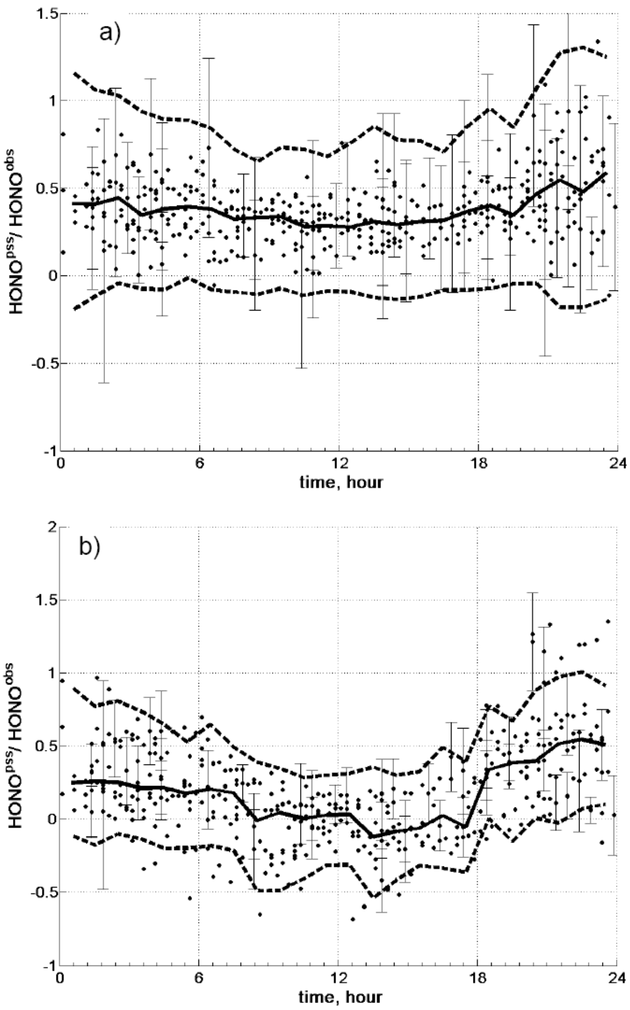

Figure 9. Ratio of calculated and measured [HONO]: **(a)** from OH budget; **(b)** from net radical (OH and RO_2) sources and sinks. Solid lines – median values; dashed lines – upper and lower quartiles of the mean values with added and subtracted standard deviation, respectively. Error bars correspond to standard deviation.

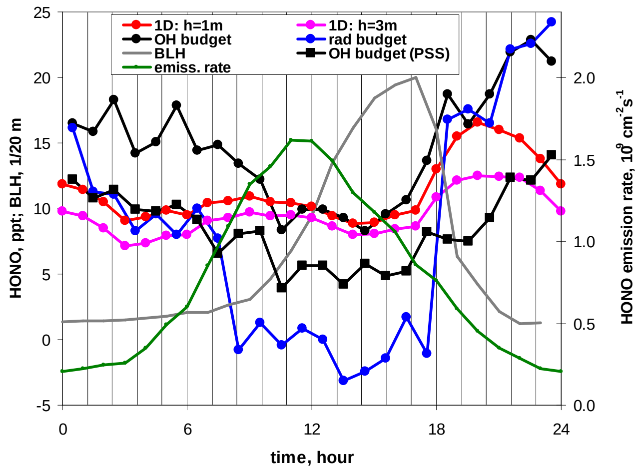

Figure 10. Comparison of median diurnal profiles of [HONO] derived from OH (black) and sum of radicals (OH and RO_2) (blue) budgets with [HONO] calculated with 1-D model at the heights of 1m (red) and 3 m (magenta) for the days 2–9 of January. Black circles and squares correspond to [HONO] derived using measured and calculated steady-state [NO_2], respectively. Grey and green lines represent modelled median boundary layer height and HONO emission rates, respectively.

tion of the concentrations of HONO using the LOPAP technique. According to Legrand et al. (2014), about 100 pptv of HO_2NO_2 may result in interference equivalent to about 15 pptv of HONO. As the interference has not yet been well characterized and, in addition, no measurements of HO_2NO_2 were available at Dome C, a correction of HONO data at Dome C is not presently possible.

As an alternative approach, we have compared the concentrations of HONO derived by examining the radical budget (Fig. 9) with the calculations assuming HONO snow emissions at Dome C estimated from the laboratory studies of Legrand et al. (2014). By irradiating the surface of snow collected at Concordia and simultaneously measuring the concentrations of HONO and NO_x produced from the snow the authors found that HONO mixing ratios in the experiment chamber outflow were roughly 30–50 % of the mixing ratio of NO_x, depending on snow temperature. Under temperature conditions encountered at Dome C the HONO / NO_x ratio ranged from 0.57 during the day (at $-25\,°C$) and 0.3 at night (at $-35\,°C$). Applying this ratio to the NO_x snow emission flux at Dome C, derived from the NO_x vertical gradients measured during the OPAL campaign by Frey et al. (this issue), Legrand et al. (2014) estimated a HONO flux at Dome C ranging from 0.2×10^9 molecules cm^{-2} s^{-1} at night to 1.5×10^9 molecules cm^{-2} s^{-1} at noon. These fluxes of HONO were used in the work described here to estimate the concentrations of HONO at different heights above the snow using the 1-D chemistry-transport box model (Sect. 2.3) with turbulent vertical transport and a simplified chemistry scheme including HONO production via the snow emissions only and HONO removal via photolysis. Formation of HONO in the reaction OH + NO contributing less than 10 % to the concentration of HONO resulting from the snow emissions was neglected in the present 1-D calculations. Another gas-phase source of HONO via reaction of $HO_2(H_2O)$ complex with NO_2 was recently proposed by Li et al. (2014). Owing to low temperatures at Dome C the contribution of this source to [HONO] is estimated to be less than 2–3 % (Legrand et al., 2014) and it was also neglected in the 1-D model.

The results of the 1-D calculations are shown in Fig. 10 where the median diurnal profiles of emission fluxes, boundary layer heights and simulated mixing ratios of HONO at 1 and 3 m are shown for the period from 19 December to 5 January. Figure 10 shows that the difference of HONO mixing ratios at 1m and 3 m does not exceed 30 % and, hence,

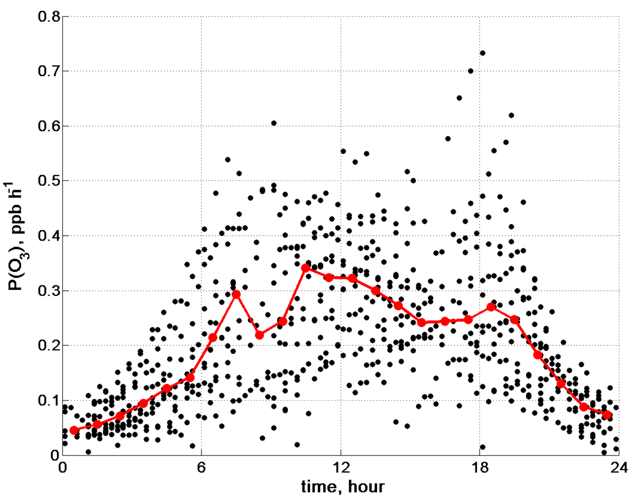

Figure 11. Ozone production calculated from measured [RO_2] and [NO]: red line represents hourly median values.

the vertical gradient of [HONO] and measurements of [OH] and [HONO] at different heights, 1 and 3 m, respectively, can only partly explain the overestimation of OH production from HONO. This conclusion does not depend on the strength of HONO flux used in the model because the relative difference between concentrations of HONO at different heights above the snowpack is determined only by the diffusivity of the boundary layer and the lifetime of HONO.

The HONO mixing ratio-time profiles calculated with the 1-D model are compared in Fig. 10 with the HONO profiles resulting from analysis of the radical budgets. The levels of HONO derived from the OH budget with measured NO_2 are about 10 pptv higher than the HONO values obtained using PSS NO_2 concentrations. In both cases the HONO mixing ratios derived from the OH budget are in reasonable agreement with [HONO] predicted by the 1-D model (within 5 pptv). The 1-D model reproduces also the diurnal HONO concentration profile with a minimum during the day and larger concentration of HONO in the evening resulting from interplay between emission rate and BL height variability (Legrand et al., 2014). For the concentrations of HONO derived from the $OH + RO_2$ budget with measured NO_2 the model significantly underestimates that derived from the budget daytime [HONO] but provides better agreement for the night and reproduces the general temporal trend of HONO variability. The concentrations of HONO derived from the $OH + RO_2$ budget with steady-state [NO_2] are negative (about −8 ppt during the day) and not presented in Fig. 10.

3.6 Ozone production

The RO_2 and NO measurements made at Dome C were used to estimate local boundary layer ozone production. As seen in Fig. 11, the peak calculated ozone production rate ($P(O_3)$) is about 0.2 ppbv h^{-1} during daytime (using the measurements of RO_2 at 3 m, NO at 4 m above the snowpack and assuming $P(O_3)$ equal to NO_2 production rate in the reaction of RO_2 with NO). The production rate is in fairly good agreement with the previous estimation of 0.2 ppbv h^{-1} derived from examination of diurnal changes in the concentration of ozone (Legrand et al., 2009). The integrated 24 h production of ozone reaches 4.7 ppbv d^{-1} at Dome C and is similar to the one calculated for the SP where the daily production of ozone was estimated from a model using measured concentrations of NO and OH to be of 2.2–3.6 ppbv d^{-1} for ISCAT 1998 (Crawford et al., 2001) and 3.2–4.8 ppbv d^{-1} for ISCAT 2000 (Chen et al., 2004).

It has to be emphasized with respect to the previous discussion of the ratio [NO_2] / [NO] observed at Dome C that if the concentration of RO_2 radical was as large as needed to explain the observed [NO_2] / [NO] ratio, the corresponding production rate of ozone would be as large as 100 ppbv d^{-1} and would strongly conflict with observed diurnal change of ozone (see Fig. 3 in Legrand et al. (2014).

4 Conclusions

Concentrations of hydroxyl radicals and the sum of peroxy radicals, RO_2, have been measured for the first time on the East Antarctic Plateau at the Concordia station (Dome C). The concentrations of OH and RO_2 radicals were found to be comparable to those observed previously at the South Pole (Mauldin et al., 2001, 2004, 2010) confirming that the elevated oxidative capacity found at the SP is not unique but a common characteristic of near-surface atmospheric layer for a large part of the high Antarctic plateau.

Similar to the findings at the SP the major explanation for the large concentrations of OH radical at Dome C was found to be the large concentrations of NO (Frey et al., 2013, 2014) leading to fast recycling of peroxy radicals to OH radicals. Also, similarly to the SP, the variability of the concentration of NO_x plays a major role in controlling the variability of radicals (OH and RO_2) at Dome C. In contrast to the SP, where there is no diurnal variation of solar radiation, and where radical levels are controlled by the concentrations of NO mostly via changing boundary layer properties (Neff et al., 2008), [OH] and [RO_2] at Dome C show strong diurnal variability correlating with the solar cycle, which in turn controls the rate of radical production and the rate of interconversion of OH and RO_2 radicals.

The large concentrations of radicals and NO result in ozone production in the BL at Dome C with a production rate of 0.1–0.3 ppb h^{-1}, similar to that observed at the SP.

The major primary sources of radicals in the atmosphere at Dome C are represented by the photolysis of HONO, HCHO, CH_3CHO and H_2O_2, (in order of decreasing significance), with photolysis of HONO deduced from measurements of HONO contributing for about 75 % of total primary production of radicals. The main net losses of radicals are represented by their reactions with NO_2 and cross radical reactions. However, it is found, that these results are inconsistent with observations of radicals leading to about a factor of 2 overestimation of the concentrations of RO_2 and OH radicals. At the same time, neglecting the production of OH radical from the photolysis of HONO results in about a factor of 2 underestimation of the measured concentrations of radicals. Based on 0-D modelling, to explain the observations of OH and RO_2 radicals, in this case an additional source of OH equivalent to about 25 % of measured photolysis of HONO is required. Similar result follows from analysis of the photochemical budget of the OH radicals for which the balance is achieved by reducing P_{HONO} by a factor of 3.

The conclusions based on the radical budget analysis and 0-D modelling using the measured concentrations of NO and NO_2 may be significantly biased because the chemical mechanism derived from the available field observations at Dome C is inconsistent with observed large ratios of [NO_2] to [NO]. Assuming that measured NO_2 mixing ratios were overestimated due to unknown interference and using instead [NO_2] estimated assuming steady-state results in lower radical losses and, hence, stronger overestimation of the radical production. In this case, based on the analysis of the radical budgets the observed concentrations of OH radicals are consistent with the levels of HONO corresponding to about (15–20) % of the measured values, while for the sum of the radicals the radical production is overestimated even neglecting the net OH source from the photolysis of HONO. Based on 0-D modelling steady-state derived NO_2, the measured OH concentrations are in agreement with steady-state HONO mixing ratios (about 1–2 pptv), while the concentrations of RO_2 radicals are overestimated by about 50 % even neglecting the net radical production by the photolysis of HONO.

Hence, in both cases corresponding to the measured or the PSS-derived concentrations of NO_2 the calculations, 0-D modelling or budget analysis, overestimate the OH and RO_2 concentrations. If this inconsistency is due to an overestimation of the concentrations of HONO, the degree of the overestimation depends on the concentrations of NO_2 used in the calculations. Using the measured NO_2 results in an overestimation of HONO by a factor of 3–4. If the concentrations of NO_2 are estimated assuming steady-state conditions the net radical production from the HONO photolysis should be reduced by a factor of 5 or completely removed based on the budget of OH or 0-D modelling, respectively.

Assuming that HONO at Dome C originates from snow emissions with the emission strength evaluated by Legrand et al. (2014) we obtain from a 1-D model the concentrations of HONO corresponding to about 20–30 % of measured [HONO] and the diurnal concentration profiles of HONO consistent with those calculated from the budget analysis of OH radicals with the concentrations of NO_2 either calculated assuming PSS or taken from the measurements. We suggest that an explanation for the overestimation of radical production could be an overestimation of measured concentration of HONO, which may originate from the measurement interference from HO_2NO_2 affecting measurements of HONO by LOPAP (Legrand et al., 2014). Even with a factor of 4 reduction in the concentrations of HONO, the photolysis of HONO represents the major primary radical source at Dome C accounting for about 45 % of primary radical production.

Considering the observed uncertainties in HONO and NO_x measurements we suggest that further studies of NO_x, HONO, peroxy nitrates (RO_2NO_2) and radical chemistry at Antarctic Plateau are required with specific efforts dedicated to increase the reliability of measurements (especially HONO and NO_2) under polar conditions.

Acknowledgements. The OPALE project was funded by the ANR (Agence National de Recherche) contract ANR-09-BLAN-0226. National financial support and field logistic supplies for the summer campaign were provided by Institut Polaire Français-Paul Emile Victor (IPEV) within programs No. 414 and 903. M. D. King and J. L. France wish to thank NERC (NE/F0004796/1 and NE/F0104788) and NERC FSF (555.0608 and 584.0609).

Edited by: J. W. Bottenheim

References

Bauguitte, S. J.-B., Bloss, W. J., Evans, M. J., Salmon, R. A., Anderson, P. S., Jones, A. E., Lee, J. D., Saiz-Lopez, A., Roscoe, H. K., Wolff, E. W., and Plane, J. M. C.: Summertime NO_x measurements during the CHABLIS campaign: can source and sink estimates unravel observed diurnal cycles?, Atmos. Chem. Phys., 12, 989–1002, doi:10.5194/acp-12-989-2012, 2012.

Berresheim, H., Elste, T., Plass-Dulmer, C., Eisele, F. L., and Tanner, D. J.: Chemical ionization mass spectrometer for long-term measurements of atmospheric OH and H_2SO_4, Int. J. Mass Spectrom., 202, 91–109, 2000.

Chen, G., Davis, D., Crawford, J., Hutterli, L. M., Huey, L. G., Slusher, D., Mauldin, L., Eisele, F., Tanner, D., Dibb, J., Buhr, M., McConnell, J., Lefer, B., Shetter, R., Blake, D., Song, C. H., Lombardi, K., and Arnoldy, J.: A reassessment of HO_x South Pole chemistry based on observations recorded during ISCAT 2000, Atmos. Environ., 38, 5451–5461, 2004.

Crawford, J. H., Davis, D. D., Chen, G., Buhr, M., Oltmans, S., Weller, R., Mauldin, L., Eisele, F., Shetter, R., Lefer, B., Arimoto, R., and Hogan, A.: Evidence for photochemical production of ozone at the South Pole surface, Geophys. Res. Lett., 28, 3641–3644, 2001.

Davis, D., Nowak, J. B., Chen, G., Buhr, M., Arimoto, R., Hogan, A., Eisele, F., Mauldin, L., Tanner, D., Shetter, R., Lefer, B., and McMurry, P.: Unexpected high levels of NO observed at South Pole, Geophys. Res. Lett., 28, 3625–3628, 2001.

Davis, D. D., Eisele, F., Chen, G., Crawford, J., Huey, G., Tanner, D., Slusher, D., Mauldin, L., Oncley, S., Lenschow, D., Semmer, S., Shetter, R., Lefer, B., Arimoto, R., Hogan, A., Grube, P., Lazzara, M., Bandy, A., Thornton, D., Berresheim, H., Bingemer, H., Hutterli, M., McConnell, J., Bales, R., Dibb, J., Buhr, M., Park, J., McMurry, P., Swanson, A., Meinardi, S., and Blake, D.:

An overview of ISCAT 2000, Atmos. Environ., 38, 5363–5373, 2004.

Davis, D. D., Seelig, J., Huey, G., Crawford, J., Chen, G., Wang, Y. H., Buhr, M., Helmig, D., Neff, W., Blake, D., Arimoto, R., and Eisele, F.: A reassessment of Antarctic plateau reactive nitrogen based on ANTO 2003 airborne and ground based measurements, Atmos. Environ., 42, 2831–2848, 2008.

Dibb, J. E., Huey, L. G., Slusher, D. L., and Tanner, D. J.: Soluble reactive nitrogen oxides at South Pole during ISCAT 2000, Atmos. Environ., 38, 5399–5409, 2004.

Dusanter, S., Vimal, D., and Stevens, P. S.: Technical note: Measuring tropospheric OH and HO_2 by laser-induced fluorescence at low pressure. A comparison of calibration techniques, Atmos. Chem. Phys., 8, 321–340, doi:10.5194/acp-8-321-2008, 2008.

Eisele, F. L. and Tanner, D. J.: Ion-Assisted Tropospheric OH Measurements, J. Geophys. Res.-Atmos., 96, 9295–9308, 1991.

Eisele, F., Davis, D. D., Helmig, D., Oltmans, S. J., Neff, W., Huey, G., Tanner, D., Chen, G., Crawford, J., Arimoto, R., Buhr, M., Mauldin, L., Hutterli, M., Dibb, J., Blake, D., Brooks, S. B., Johnson, B., Roberts, J. M., Wang, Y. H., Tan, D., and Flocke, F.: Antarctic Tropospheric Chemistry Investigation (ANTCI) 2003 overview, Atmos. Environ., 42, 2749–2761, 2008.

Faloona, I. C., Tan, D., Lesher, R. L., Hazen, N. L., Frame, C. L., Simpas, J. B., Harder, H., Martinez, M., Di Carlo, P., Ren, X. R., and Brune, W. H.: A laser-induced fluorescence instrument for detecting tropospheric OH and HO_2: Characteristics and calibration, J. Atmos. Chem., 47, 139–167, 2004.

France, J. L., King, M. D., Frey, M. M., Erbland, J., Picard, G., Preunkert, S., MacArthur, A., and Savarino, J.: Snow optical properties at Dome C (Concordia), Antarctica; implications for snow emissions and snow chemistry of reactive nitrogen, Atmos. Chem. Phys., 11, 9787–9801, doi:10.5194/acp-11-9787-2011, 2011.

Frey, M. M., Stewart, R. W., McConnell, J. R., and Bales, R. C.: Atmospheric hydroperoxides in West Antarctica: Links to stratospheric ozone and atmospheric oxidation capacity, J. Geophys. Res.-Atmos., 110, D23301, doi:10.1029/2005JD006110, 2005.

Frey, M. M., Brough, N., France, J. L., Anderson, P. S., Traulle, O., King, M. D., Jones, A. E., Wolff, E. W., and Savarino, J.: The diurnal variability of atmospheric nitrogen oxides (NO and NO2) above the Antarctic Plateau driven by atmospheric stability and snow emissions, Atmos. Chem. Phys., 13, 3045–3062, doi:10.5194/acp-13-3045-2013, 2013.

Frey, M. M., Roscoe, H. K., Kukui, A., Savarino, J., France, J. L., King, M. D., Legrand, M., and Preunkert, S.: Atmospheric nitrogen oxides (NO and NO_2) at Dome C, East Antarctica, during the OPALE campaign, Atmos. Chem. Phys. Discuss., in preparation, 2014.

Fuchs, H., Holland, F., and Hofzumahaus, A.: Measurement of tropospheric RO_2 and HO_2 radicals by a laser-induced fluorescence instrument, Rev. Sci. Instrum., 79, 084104, doi:10.1063/1.2968712, 2008.

Gallée, H. and Gorodetskaya, I.: Validation of a limited area model over Dome C, Antarctic Plateau, during winter, 34, 61–72, Clim. Dynam., doi:10.1007/s00382-008-0499-y, 2008.

Gallée, H., Preunkert, S., Argentini, S., Frey, M. M., Genthon, C., Jourdain, B., Pietroni, I., Casasanta, G., Barral, H., Vignon, E., and Legrand, M.: Characterization of the boundary layer at Dome C (East Antarctica) during the OPALE summer campaign, Atmos. Chem. Phys. Discuss., in preparation, 2014.

Grannas, A. M., Jones, A. E., Dibb, J., Ammann, M., Anastasio, C., Beine, H. J., Bergin, M., Bottenheim, J., Boxe, C. S., Carver, G., Chen, G., Crawford, J. H., Dominé, F., Frey, M. M., Guzmán, M. I., Heard, D. E., Helmig, D., Hoffmann, M. R., Honrath, R. E., Huey, L. G., Hutterli, M., Jacobi, H. W., Klán, P., Lefer, B., McConnell, J., Plane, J., Sander, R., Savarino, J., Shepson, P. B., Simpson, W. R., Sodeau, J. R., von Glasow, R., Weller, R., Wolff, E. W., and Zhu, T.: An overview of snow photochemistry: evidence, mechanisms and impacts, Atmos. Chem. Phys., 7, 4329–4373, doi:10.5194/acp-7-4329-2007, 2007.

Hamer, P. D., Shallcross, D. E., and Frey, M. M.: Modelling the impact of oxygenated VOC and meteorology upon the boundary layer photochemistry at the South Pole, Atmos. Sci. Let., 8, 14–20, 2007.

Hanke, M., Uecker, J., Reiner, T., and Arnold, F.: Atmospheric peroxy radicals: ROXMAS, a new mass-spectrometric methodology for speciated measurements of HO_2 and Sigma RO_2 and first results, Int. J. Mass Spectrom., 213, 91–99, 2002.

Heard, D. E. and Pilling, M. J.: Measurement of OH and HO_2 in the troposphere, Chem. Rev., 103, 5163–5198, 2003.

Heland, J., Kleffmann, J., Kurtenbach, R., and Wiesen, P.: A new instrument to measure gaseous nitrous acid (HONO) in the atmosphere, Environ. Sci. Technol., 35, 3207–3212, doi:10.1021/es000303t, 2001.

Honrath, R. E., Peterson, M. C., Guo, S., Dibb, J. E., Shepson, P. B., and Campbell, B.: Evidence of NO_x production within or upon ice particles in the Greenland snowpack, Geophys. Res. Lett., 26, 695–698, 1999.

Jäkel, E., Wendisch, M., Blumthaler, M., Schmitt, R., and Webb, A. R.: A CCD Spectroradiometer for Ultraviolet Actinic Radiation Measurements, J. Atmos. Ocean. Technol. 24, 449–462, 2007.

Jenkin, M. E., Saunders, S. M., and Pilling, M. J.: The tropospheric degradation of volatile organic compounds: A protocol for mechanism development, Atmos. Environ., 31, 81–104, 1997.

Jones, A. E., Weller, R., Anderson, P. S., Jacobi, H. W., Wolff, E. W., Schrems, O., and Miller, H.: Measurements of NO_x emissions from the Antarctic snowpack, Geophys. Res. Lett., 28, 1499–1502, 2001.

Kerbrat, M., Legrand, M., Preunkert, S., Gallee, H., and Kleffmann, J.: Nitrous acid at Concordia (inland site) and Dumont d'Urville (coastal site), East Antarctica, J. Geophys. Res.-Atmos., 117, D08303, doi:10.1029/2011JD017149, 2012.

King, J. C., Argentini, S. A., and Anderson, P. S.: Contrasts between the summertime surface energy balance and boundary layer structure at Dome C and Halley stations, Antarctica, J. Geophys. Res.-Atmos., 111, D02105, doi:10.1029/2005JD006130, 2006.

Kleffmann, J., Heland, J., Kurtenbach, R., Lorzer, J., and Wiesen, P.: A new instrument (LOPAP) for the detection of nitrous acid (HONO), Environ. Sci. Pollut. Res., 4, 48–54, 2002.

Kukui, A., Ancellet, G., and Le Bras, G.: Chemical ionisation mass spectrometer for measurements of OH and Peroxy radical concentrations in moderately polluted atmospheres, J. Atmos. Chem., 61, 133–154, 2008.

Kukui, A., Legrand, M., Ancellet, G., Gros, V., Bekki, S., Sarda-Esteve, R., Loisil, R., and Preunkert, S.: Measurements of OH and RO_2 radicals at the coastal Antarctic site of Dumont d'Urville (East Antarctica) in summer 2010–2011, J. Geophys. Res.-Atmos., 117, D12310, doi:10.1029/2012JD017614, 2012.

Legrand, M., Preunkert, S., Jourdain, B., Gallee, H., Goutail, F., Weller, R., and Savarino, J.: Year-round record of surface ozone at coastal (Dumont d'Urville) and inland (Concordia) 20 sites in East Antarctica, J. Geophys. Res.-Atmos., 114, D20306, doi:10.1029/2008JD011667, 2009.

Legrand, M., Gros, V., Preunkert, S., Sarda-Estève, R., Thierry, A.-M., Pépy, G., and Jourdain, B.: A reassessment of the budget of formic and acetic acids in the boundary layer at Dumont d'Urville (coastal Antarctica): The role of penguin emissions on the budget of several oxygenated volatile organic compounds, J. Geophys. Res.-Atmos., 117, D06308, doi:10.1029/2011JD017102, 2012.

Legrand, M., Preunkert, S., Frey, M., Bartels-Rausch, T., Kukui, A., King, M., Kerbrat, M, Jourdain, B., and Savarino, J: High atmospheric levels of nitrous acid at Concordia (East Antarctic plateau) in summer: a strong source from surface snow?, Atmos. Chem. Phys., 14, 9963–9976, doi:10.5194/acp-14-9963-2014, 2014.

Li, X., Rohrer, F., Hofzumahaus, A., Brauers, T., Häseler, R., Bohn, B., Broch, S., Fuchs, H., Gomm, S., Holland, F., Jäger, J., Kaiser, J., Keutsch, F. N., Lohse, I., Lu, K., Tillmann, R., Wegener, R., Wolfe, G. M., Mentel, T. F., Kiendler-Scharr, A., and Wahner, A.: Missing Gas-Phase Source of HONO Inferred from Zeppelin Measurements in the Troposphere, Science, 344, 292–296, 2014.

Liao, J., Huey, L. G., Tanner, D. J., Brough, N., Brooks, S., Dibb, J. E., Stutz, J., Thomas, J. L., Lefer, B., Haman, C., and Gorham, K.: Observations of hydroxyl and peroxy radicals and the impact of BrO at Summit, Greenland in 2007 and 2008, Atmos. Chem. Phys., 11, 8577–8591, doi:10.5194/acp-11-8577-2011, 2011.

Madronich, S.: Photodissociation in the atmosphere 1. Actinic flux and the effects of ground reflectance and clouds, J. Geophys. Res., 92, 9740–9752, 1987.

Mauldin, R. L., Eisele, F. L., Tanner, D. J., Kosciuch, E., Shetter, R., Lefer, B., Hall, S. R., Nowak, J. B., Buhr, M., Chen, G., Wang, P., and Davis, D.: Measurements of OH, H_2SO_4, and MSA at the South Pole during ISCAT, Geophys. Res. Lett., 28, 3629–3632, 2001.

Mauldin, R. L., Kosciuch, E., Henry, B., Eisele, F. L., Shetter, R., Lefer, B., Chen, G., Davis, D., Huey, G., and Tanner, D.: Measurements of OH, $HO_2 + RO_2$, H_2SO_4, and MSA at the south pole during ISCAT 2000, Atmos. Environ., 38, 5423–5437, 2004.

Mauldin, R., Kosciuch, E., Eisele, F., Huey, G., Tanner, D., Sjostedt, S., Blake, D., Chen, G., Crawford, J., and Davis, D.: South Pole Antarctica observations and modeling results: New insights on HO_x radical and sulfur chemistry, Atmos. Environ., 44, 572–581, 2010.

Michoud, V., Kukui, A., Camredon, M., Colomb, A., Borbon, A., Miet, K., Aumont, B., Beekmann, M., Durand-Jolibois, R., Perrier, S., Zapf, P., Siour, G., Ait-Helal, W., Locoge, N., Sauvage, S., Afif, C., Gros, V., Furger, M., Ancellet, G., and Doussin, J. F.: Radical budget analysis in a suburban European site during the MEGAPOLI summer field campaign, Atmos. Chem. Phys., 12, 11951–11974, doi:10.5194/acp-12-11951-2012, 2012.

Neff, W., Helmig, D., Grachev, A., and Davis, D.: A study of boundary layer behavior associated with high NO concentrations at the South Pole using a minisodar, tethered balloons and sonic anemometer, Atmos. Environ., 42, 2762–2779, 2008.

Novelli, P. C. and Masarie, K. A.: Atmospheric Carbon Monoxide Dry Air Mole Fractions from the NOAA ESRL Carbon Cycle Cooperative Global Air Sampling Network, 1988–2012, Version: 2013-06-18, Path: ftp://aftp.cmdl.noaa.gov/data/trace_gases/co/flask/surface/ (last access: 10 August 2013), 2013.

Preunkert, S., Ancellet, G., Legrand, M., Kukui, A., Kerbrat, M., Sarda-Esteve, R., Gros, V., and Jourdain, B.: Oxidant Production over Antarctic Land and its Export (OPALE) project: an overview of the 2010–2011 summer campaign, J. Geophys. Res.-Atmos., 117, D15307, doi:10.1029/2011JD017145, 2012.

Preunkert, S., Legrand, M., Frey, M., Kukui, Savarino, J., A., Gallée, H., King, M., Jourdain, B., Vicars, W., and Helmig, D.: Formaldehyde (HCHO) in air, snow, and interstitial air at Concordia (East Antarctic plateau) in summer, Atmos. Chem. Phys. Discuss., in preparation, 2014.

Reiner, T., Hanke, M., and Arnold, F.: Atmospheric peroxy radical measurements by ion molecule reaction mass spectrometry: A novel analytical method using amplifying chemical conversion to sulfuric acid, J. Geophys. Res.-Atmos., 102, 1311–1326, 1997.

Sander, S. P., Abbatt, J., Barker, J. R., Burkholder, J. B., Friedl, R. R., Golden, D. M., Huie, R. E., Kolb, C. E., Kurylo, M. J., Moortgat, G. K., Orkin, V. L., and Wine, P. H.: Chemical Kinetics and photochemical Data for Use in Atmospheric Studies, Evaluation No. 17, JPL Publication 10-6, Jet Propulsion Laboratory, Pasadena, http://jpldataeval.jpl.nasa.gov, (last access: 10 June 2012), 2011.

Saunders, S. M., Jenkin, M. E., Derwent, R. G., and Pilling, M. J.: Protocol for the development of the Master Chemical Mechanism, MCM v3 (Part A): tropospheric degradation of non-aromatic volatile organic compounds, Atmos. Chem. Phys., 3, 161–180, doi:10.5194/acp-3-161-2003, 2003.

Sjostedt, S. J., Huey, L. G., Tanner, D. J., Peischl, J., Chen, G., Dibb, J. E., Lefer, B., Hutterli, M. A., Beyersdorf, A. J., Blake, N. J., Blake, D. R., Sueper, D., Ryerson, T., Burkhart, J., and Stohl, A.: Observations of hydroxyl and the sum of peroxy radicals at Summit, Greenland during summer 2003, Atmos. Environ., 41, 5122–5137, 2007.

Slusher, D. L., Huey, L. G., Tanner, D. J., Chen, G., Davis, D. D., Buhr, M., Nowak, J. B., Eisele, F. L., Kosciuch, E., Mauldin, R. L., Lefer, B. L., Shetter, R. E., and Dibb, J. E.: Measurements of pernitric acid at the South Pole during ISCAT 2000, Geophys. Res. Lett., 29, 2011, doi:10.1029/2002GL015703, 2002.

Slusher, D. L., Neff, W. D., Kim, S., Huey, L. G., Wang, Y., Zeng, T., Tanner, D. J., Blake, D. R., Beyersdorf, A., Lefer, B. L., Crawford, J. H., Eisele, F. L., Mauldin, R. L., Kosciuch, E., Buhr, M. P., Wallace, H. W., and Davis, D. D.: Atmospheric chemistry results from the ANTCI 2005 Antarctic plateau airborne study, J. Geophys. Res.-Atmos., 115, D07304, doi:10.1029/2009JD012605, 2010.

Steele, L. P., Krummel, P. B., and Langenfelds, R. L.: Atmospheric CH_4 concentrations from sites in the CSIRO Atmospheric Research GASLAB air sampling network (October 2002 version), in: Trends: a Compendium of Data on Global Change, Carbon Dioxide Information Analysis Center, Oak Ridge National Laboratory, US Department of Energy, Oak Ridge, TN, USA,TS15, available at: http://cdiac.esd.ornl.gov/trends/atm_meth/csiro/csiro-spoch4.html (last access: 10 August 2013), 2002.

Steele, L. P., Krummel, P. B., and Langenfelds, R. L.: Atmospheric H_2 concentrations from sites in the CSIRO Atmospheric Research GASLAB air sampling network (October 2002 version), in: Trends: a Compendium of Data on Global Change, Carbon Dioxide Information Analysis Center, Oak Ridge National Laboratory, US Department of Energy, Oak Ridge, TN, USA, available at: http://cdiac.esd.ornl.gov/trends/otheratg/csiro-h2/csiro-spoh2.html (last access: 10 August 2013), 2003.

Tanner, D. J., Jefferson, A., and Eisele, F. L.: Selected ion chemical ionization mass spectrometric measurement of OH, J. Geophys. Res.-Atmos., 102, 6415–6425, 1997.

Wang, Y. H., Choi, Y., Zeng, T., Davis, D., Buhr, M., Huey, L. G., and Neff, W.: Assessing the photochemical impact of snow NO_x emissions over Antarctica during ANTCI 2003, Atmos. Environ., 41, 3944–3958, 2007.